Supplementary Information

Immunological conversion of solid tumors using a bispecific nanobioconjugate for cancer immunotherapy

Yifei Lu[1,4,#], Kristin Huntoon[1,4,#], DaeYong Lee[1,4,#], Yifan Wang[2,#], Jonghoon Ha[2], Yaqing Qie[1,4], Xuefeng Li[2], Benjamin Schrank[2], Shiyan Dong[2], Thomas D. Gallup[1], MinJeong Kang[2], Hai Zhao[1,4], Yi An[3], Zhaogang Yang[3], Jing Li[2], Betty Y. S. Kim[1,4,*], Wen Jiang[2,*]

[1]Departments of Neurosurgery, The University of Texas MD Anderson Cancer Center, Houston, TX 77030, USA

[2]Department of Radiation Oncology, The University of Texas MD Anderson Cancer Center, Houston, TX 77030, USA

[3]Department of Therapeutic Radiology, Yale-New Haven Hospital, New Haven, CT, USA

[4]Brain Tumor Center, The University of Texas MD Anderson Cancer Center, Houston, TX 77030, USA

*Correspondence: Betty Y. S. Kim, bykim@mdanderson.org; or Wen Jiang, wjiang4@mdanderson.org

[#]These authors contributed equally

This file includes:

A

NP Group	Hydrodynamic diameter (nm)	Zeta potential (mV)	PDI
NP alone	77.28±0.38	-17.0±1.53	0.098±0.007
HER2-NP	82.56±1.53	-3.50±1.12	0.324±0.005
SLAMF7-NP	81.35±0.76	-5.34±0.17	0.212±0.010
$BiTN_{HER}$	82.57±1.45	-3.63±0.59	0.264±0.030

B

HER:SLAMF7	Anti-HER2 Ab	SLAMF7
100:0	450.0±4.4	-
75:25	360.8±9.7	522.5±4.5
50:50	250.8±7.5	1085.1±1.5
25:75	143.7±1.3	1563.7±2.7
0:100	-	2038.6±5.6

C

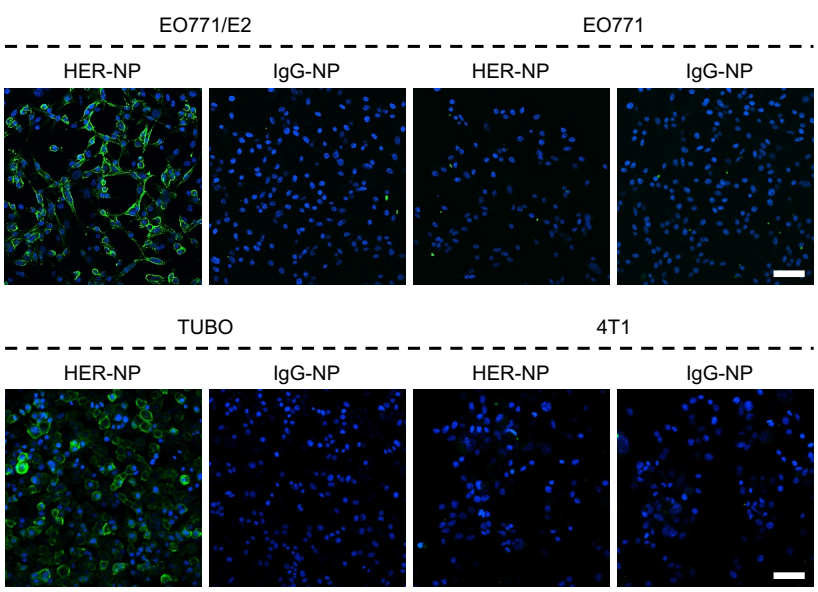

Figure S1. Nanoparticle characterization. (A) Size and zeta potential measured by dynamic light scattering (n=3). (B) Valency of $BiTN_{HER}$. The left column indicates the molecular ratio of anti-HER2 antibody and SLAMF7 added into the conjugation reaction; the right two columns indicates the number of copies of anti-HER2 antibody and SLAMF7 per nanoparticle (n=3). (C) HER-NP showed specific binding with the HER2/neu^{high} mouse breast cancer cell lines EO771/E2 and TUBO, compared with HER2/neu^{low} EO771 and 4T1 cells. (Scale bar, 50 μm).

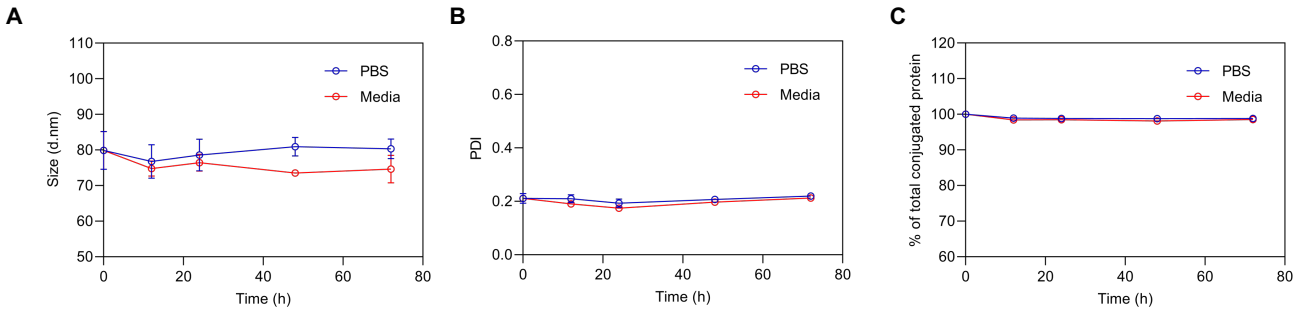

Figure S2. Stability of BiTN$_{HER}$. No significant change of nanoparticle size (A), PDI (B) and loaded protein (C) was observed in PBS or FBS-containing media within 72 hours. Data are presented as mean±s.e.m. (n=3)

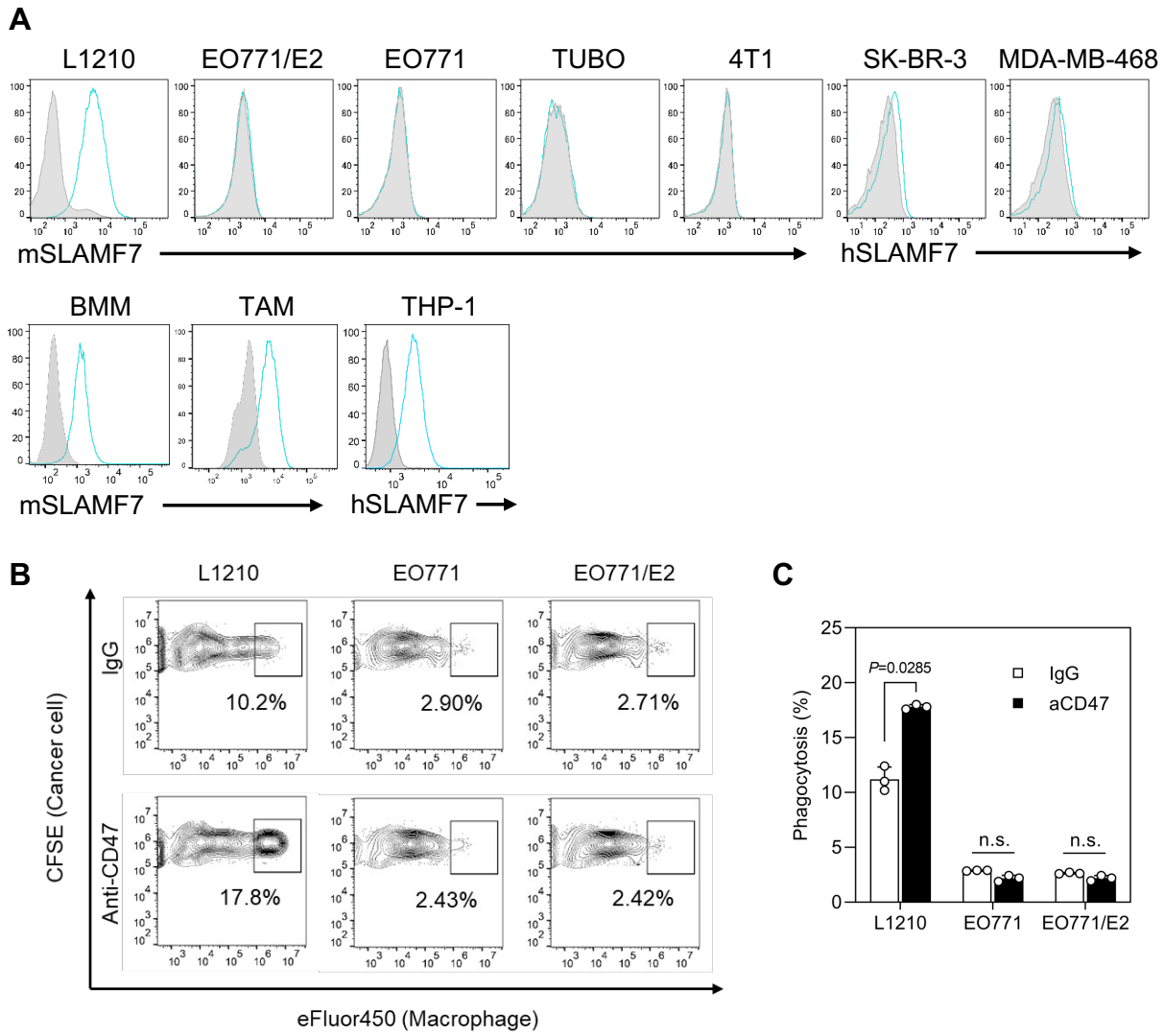

Figure S3. SLAMF7 expression and efficiency in promoting phagocytosis. (A) SLAMF7 was highly expressed on the hematopoietic mouse leukemia cell line L1210 and on mouse bone marrow–derived macrophage (BMDMs), mouse tumor-associated macrophages (TAM), and the human macrophage cell line THP-1, but was not expressed on other mouse or human breast cancer cell lines. (B,C) SLAMF7^{high} L1210 cells were more sensitive to anti-CD47 antibody–mediated macrophage phagocytosis, compared with the SLAMF7^{neg} breast cancer cell lines EO771 or EO771/E2. Data are presented as mean±s.e.m. (n=3); **P*<0.05 by two-sided unpaired Student's *t* test for the indicated comparisons; n.s., not significant.

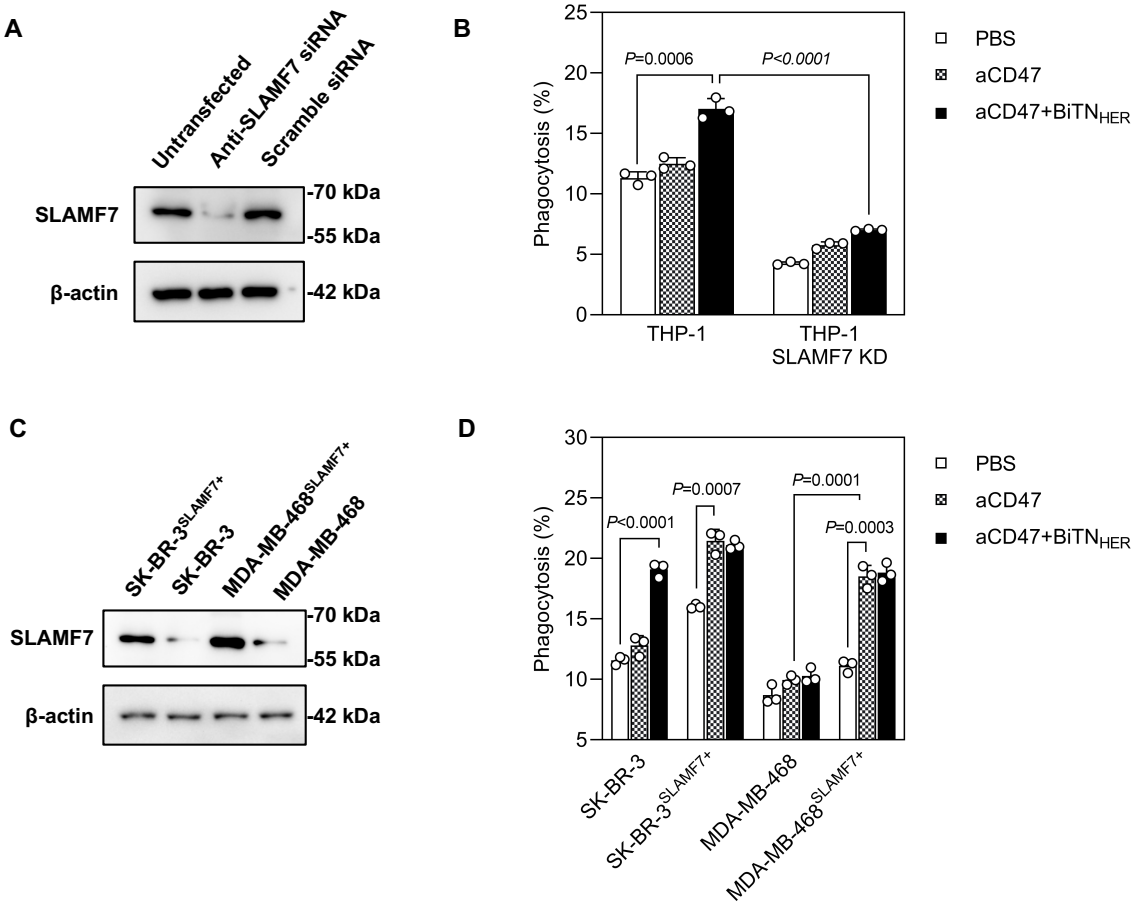

Figure S4. SLAMF7 is essential for BiTN-mediated macrophage phagocytosis of HER2^{high} cancer cells. (A) Western blotting confirmed the knock-down of SLAMF7 in THP-1 via siRNA silencing. (B) Knock-down of SLAMF7 significantly abrogated the enhancement of macrophage phagocytosis against SK-BR-3 cancer cells (n=3). (C) Western blotting confirmed the overexpression of SLAMF7 on SK-BR-3 and MDA-MB-468 via plasmid transfection. (D) SK-BR-3$^{SLAMF7+}$ and MDA-MB-468$^{SLAMF7+}$ were both susceptible to macrophage phagocytosis by CD47 blockade (n=3). Data are presented as mean±s.e.m.; **P*<0.05, ***P*<0.01, ****P*<0.001, *****P*<0.0001 by unpaired Student's *t*-test for the indicated comparisons; n.s., not significant.

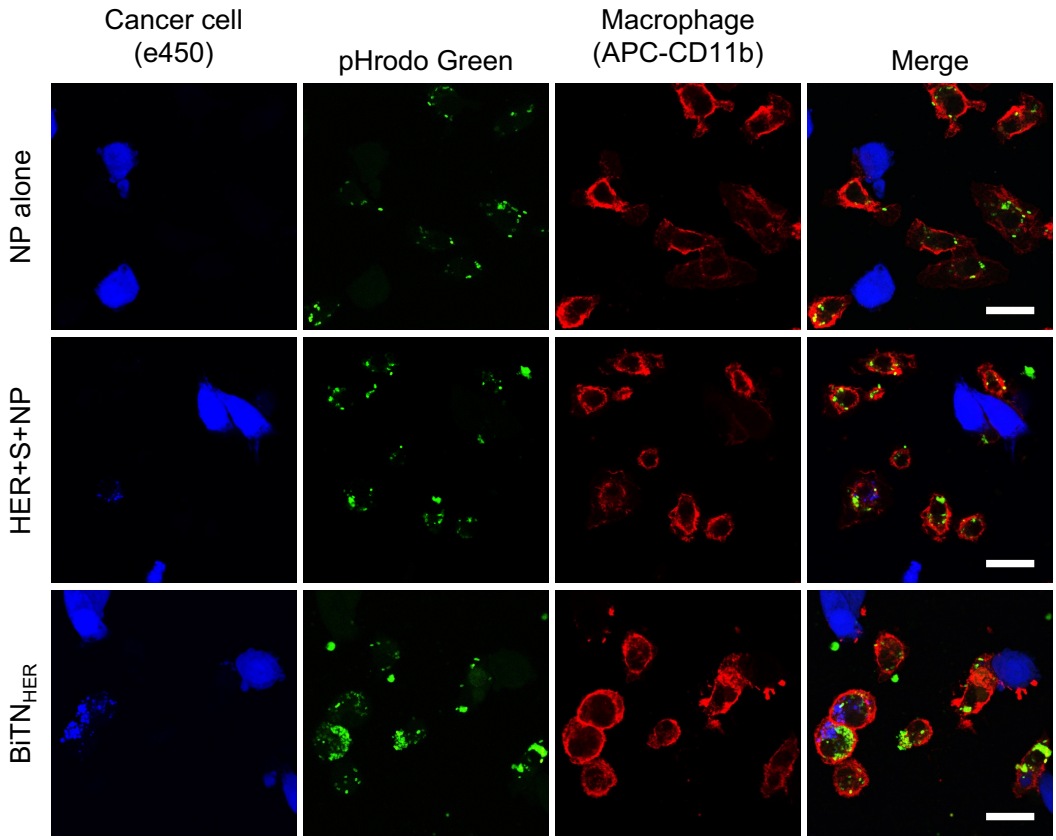

Figure S5. pHrodo assay further confirmed BiTN$_{HER}$ induced phagocytosis of EO771/E2 cancer cells. Confocal imaging showed colocalization of phagocytosed cancer cell (blue) and pHrodo bioparticles (green) in same macrophages, confirming the results of phagocytosis. Arrow heads indicate the macrophages phagocytosing both cancer cells and pHrodo bioparticles. (Scale bar, 20 μm) Experiment was repeated twice with similar results between repeats.

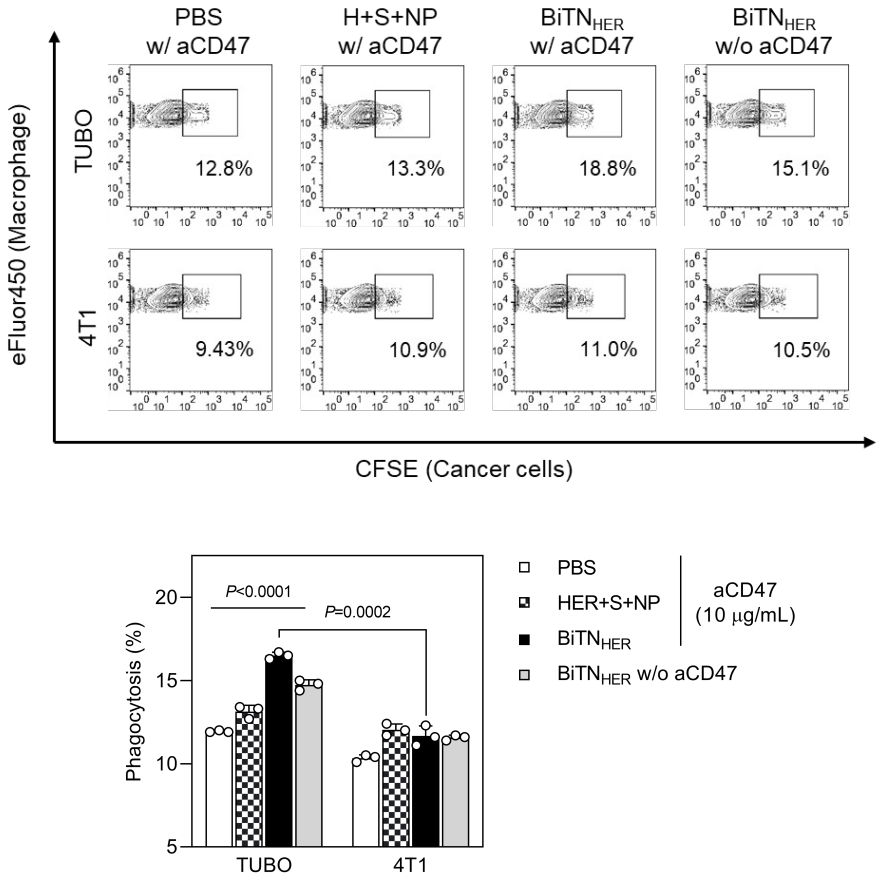

Figure S6. BiTN$_{HER}$ (with aCD47) induced macrophage phagocytosis in two different cancer cell lines. Combination treatment with BiTN$_{HER}$ and aCD47 led to a significantly greater degree of phagocytosis of HER2/neu^{high} TUBO cells compared with HER2/neu^{low} 4T1 cells. Data are presented as mean±s.e.m. (n=3); ****P < 0.0001 by one-way ANOVA; ***P < 0.001 by unpaired t test.

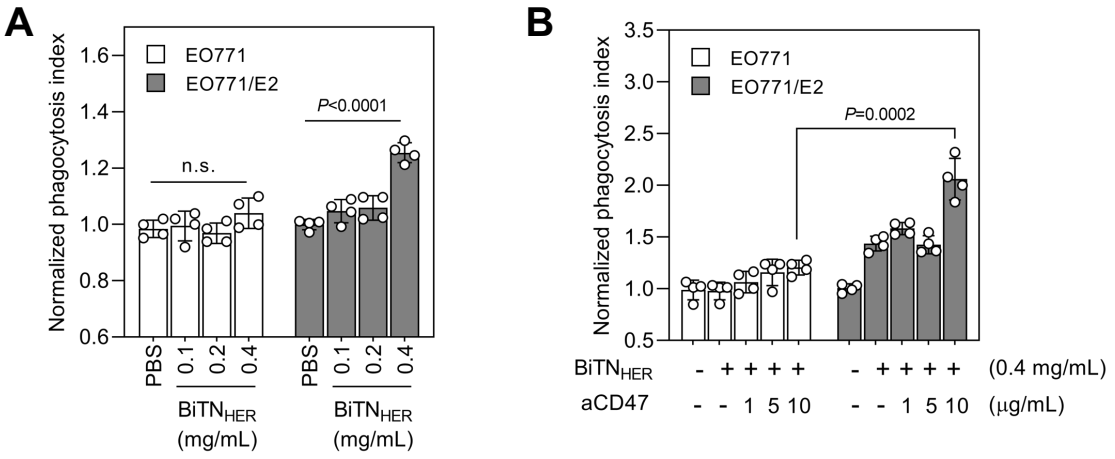

Figure S7. BiTN$_{HER}$ sensitized HER2^{high} cancer cells to CD47 blockade. (A) Macrophage phagocytosis of HER2-positive EO771/E2 cells increased with increasing concentrations of BiTN$_{HER}$. (B) The combination of BiTN$_{HER}$ and aCD47 induced a greater degree of phagocytosis of HER2-positive EO771/E2 cells when cells were pretreated with 0.4 mg/mL BiTN$_{HER}$ and 10 μg/mL aCD47. Data are presented as mean±s.e.m. (n=4); ****P < 0.0001 by one-way ANOVA; ***P<0.001 by unpaired Student's t test for the indicated comparisons; n.s., not significant.

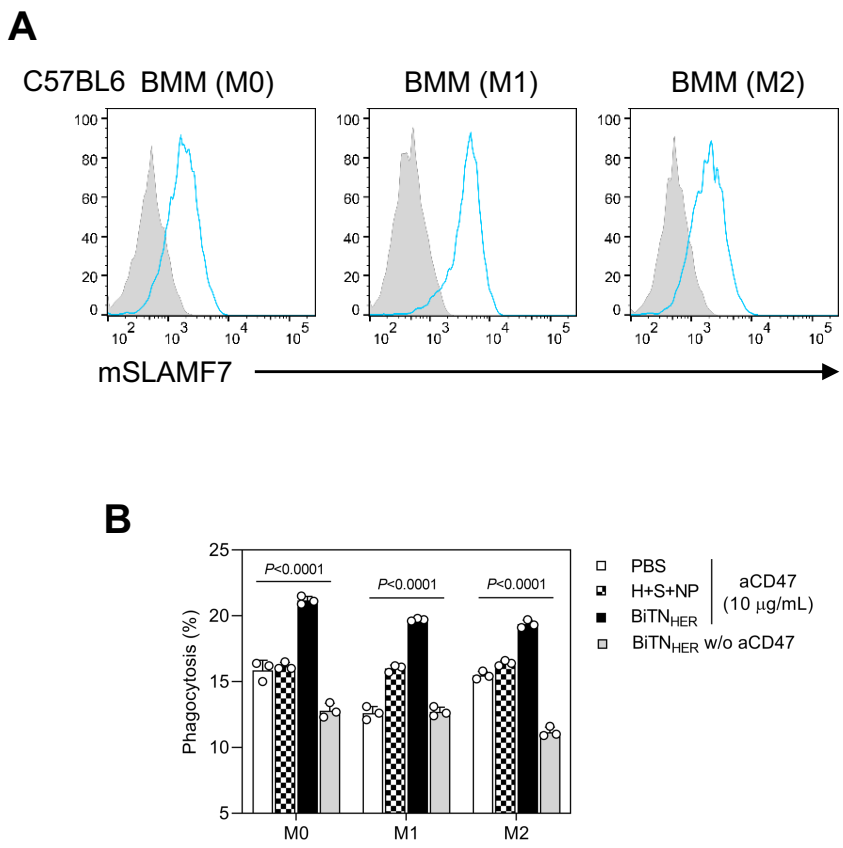

Figure S8. The polarization phenotype of macrophages resulted in similar levels of phagocytosis of HER2^{high} EO771/E2 cells. Bone marrow–derived macrophages (BMM) were polarized with lipopolysaccharide to induce M1 polarization and with IL-4 to induce M2 polarization. (A) Polarization did not affect the expression level of SLAMF7 on macrophages. (B) Polarization of macrophages did not affect macrophage phagocytosis of HER2^{high} EO771/E2 cells via the combination treatment of BiTN$_{HER}$ and aCD47. Data are presented as mean±s.e.m. (n=3). ****P < 0.0001 by one-way ANOVA.

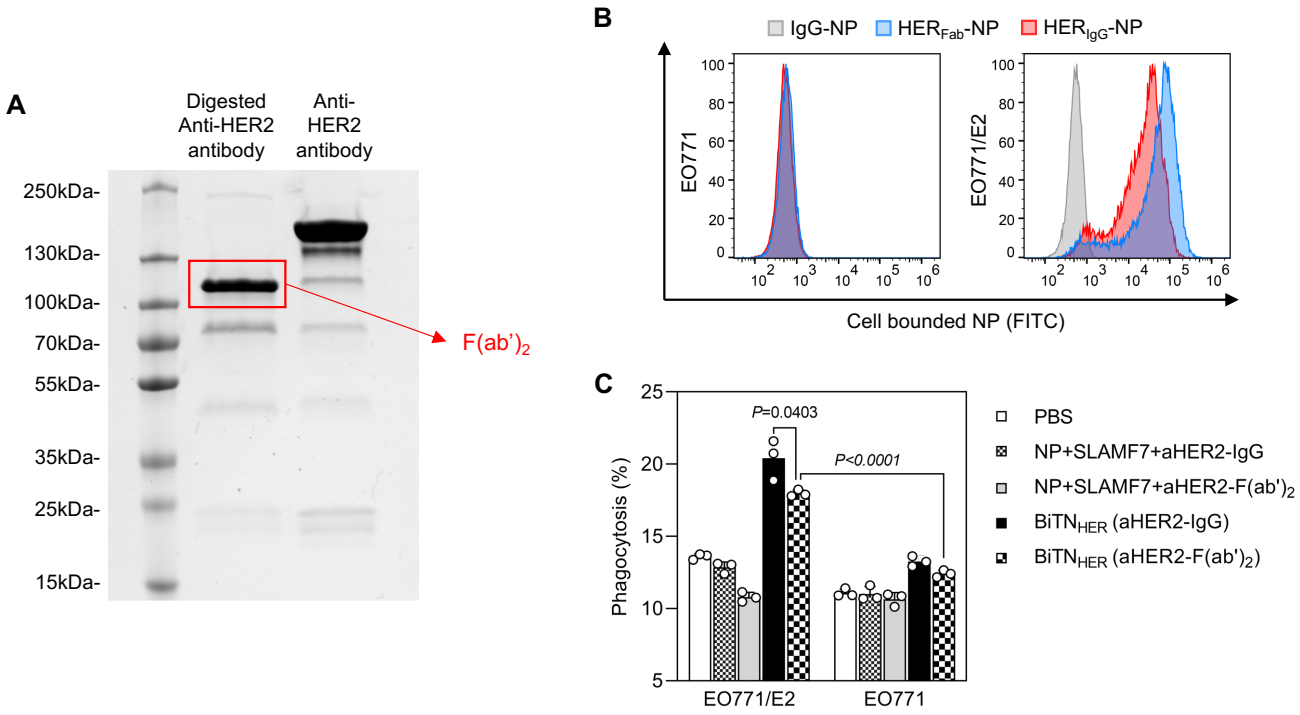

Figure S9. BiTN$_{HER}$ induced phagocytosis is not dependent on FcR engagement. a, SDS-PAGE analysis of Fc fragment digestion and F(ab')$_2$ generation from anti-HER2 antibody. Red line indicated the band of F(ab')$_2$ around 110 kDa; **b**, Purified F(ab')$_2$ fragment of anti-HER2 antibody had similar binding affinity to HER2-overexpressing EO771/E2 cells; **c**, BMDM phagocytosis of HER2^{low} EO771 and HER2^{high} EO771/E2 mouse breast cancer cells in the presence of aCD47 after treatment with PBS, NP with unconjugated anti-HER2 antibody (IgG or F(ab')$_2$ fragment) and SLAMF7,or BiTN$_{HER}$ conjugated with anti-HER2 antibody (IgG or F(ab')$_2$ fragment), (n=3). **P*<0.05, *****P*<0.0001 by unpaired Student *t* test for the indicated comparisons.

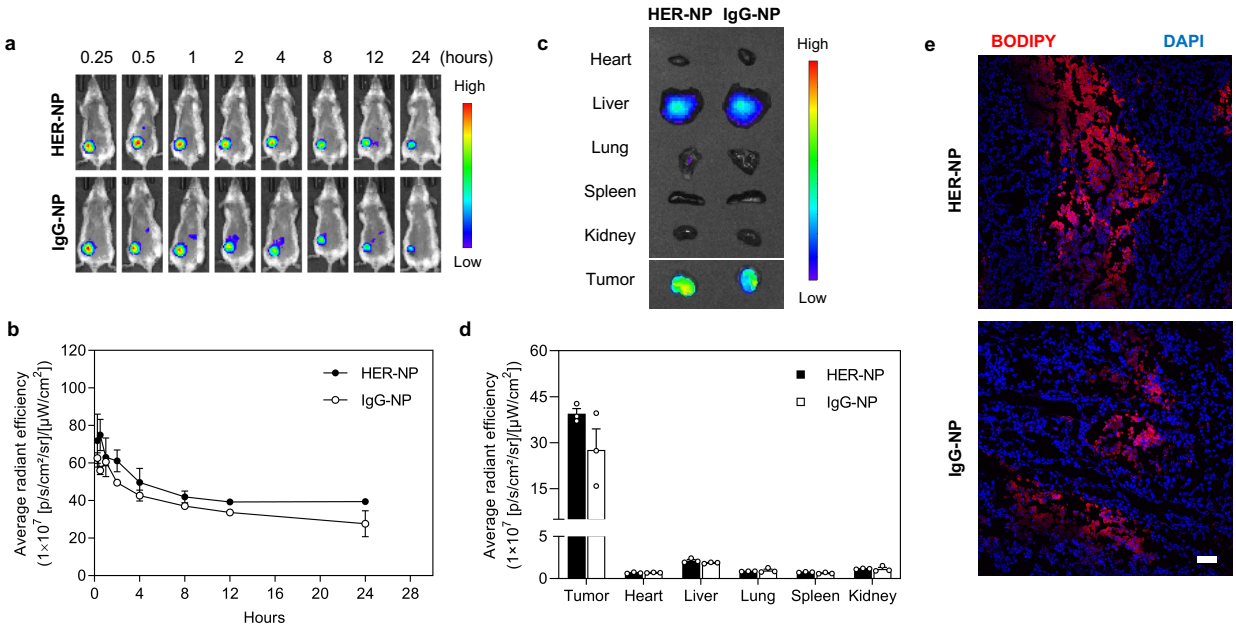

Figure S10. Biodistribution of HER-NP showed little accumulation into other major organs after intratumoral (i.t.) injection, IgG-NP was used as a non-tumor targeting control group. a, IVIS imaging of mice after i.t. injection of BODIPY-loaded nanoparticles; b, Tumor signal decline over time after i.t. injection (n=3); c, Ex vivo imaging of major organs 24 hours after i.t. injection; d, Quantitive measurement of NP signals in major organs 24 hours after i.t. injection (n=3); e, Confocal imaging of intratumoral distribution of BODIPY-labeled nanoparticles, (Red, BODIPY; Blue, DAPI. Scale bar, 50 μm). Data are presented as mean±s.e.m. (n=3)

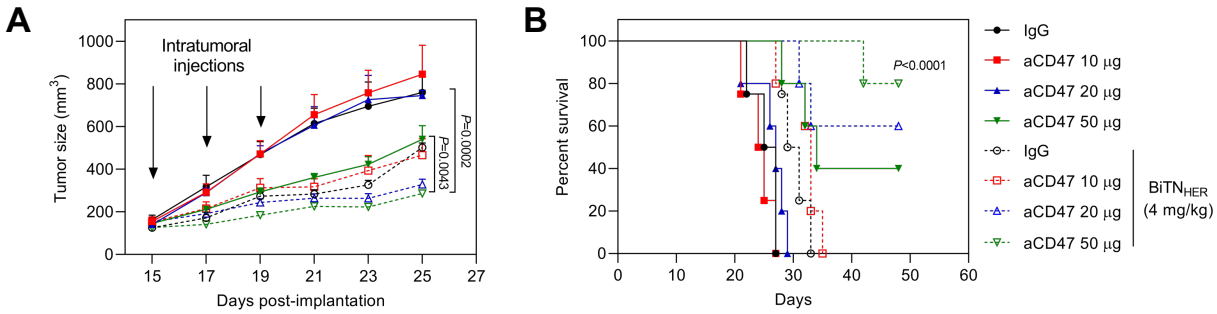

Figure S11. Determining the optimal dose of aCD47 for TUBO tumor-bearing BALB/c mice. Although $BiTN_{HER}$ in combination with either 20 μg or 50 μg aCD47 showed significant tumor inhibition (A), mouse survival was prolonged when the aCD47 dose was 50 μg (B). The $BiTN_{HER}$ dose was normalized as 4 mg/kg, and mouse IgG was used as a negative control for aCD47. Therefore, 4 mg/kg $BiTN_{HER}$ plus 50 μg aCD47 was selected for all *in vivo* experiments. Data are presented as mean±s.e.m. (n=5). $^{**}P < 0.01$, $^{***}P < 0.001$ by unpaired Student's *t* test; $^{****}P<0.0001$, log-rank test.

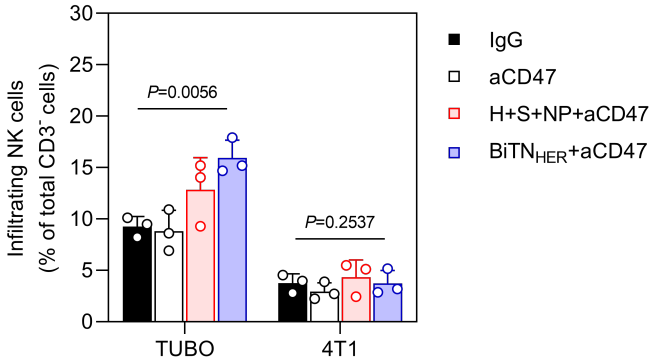

Figure S12. Combined treatment of $BiTN_{HER}$ and aCD47 promoted the infiltration of NK cells within TUBO tumors compared with 4T1 tumors (n=3). Data are presented as mean±s.d.; $^{**}P<0.01$ by one-way ANOVA with a Bonferroni *post hoc* correction; $P>0.05$ was considered as not significant.

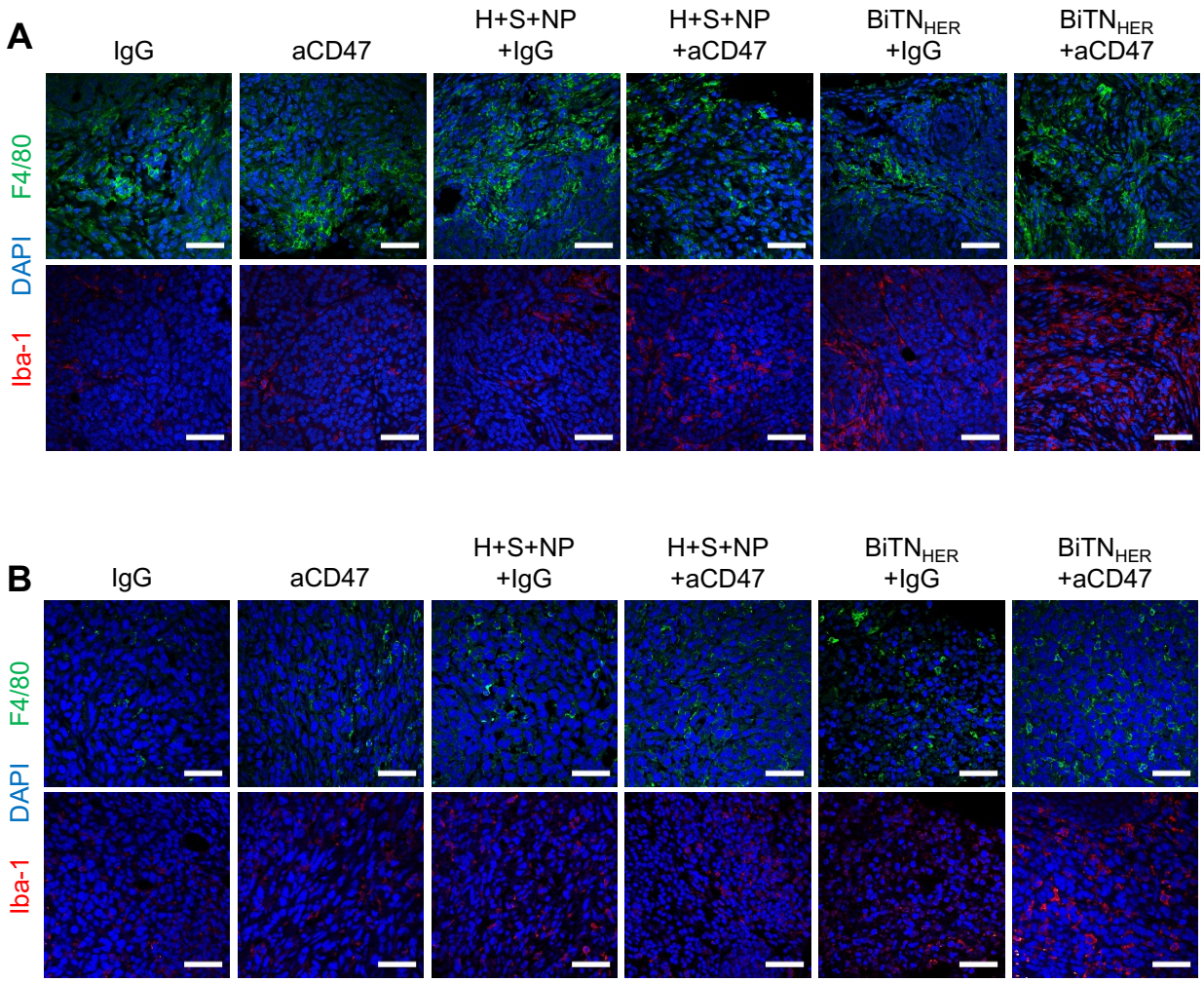

Figure S13. Combined treatment with BiTN$_{HER}$ and aCD47 induced macrophage activation in a HER2-dependent manner. (A) Combination treatment did not alter the number of intratumoral F4/80^{+} macrophages but significantly increased the number of Iba-1^{+} activated macrophages in HER2/neu^{high} TUBO breast tumors. (B) Combination treatment slightly increased the number of infiltrated macrophages and their activation in HER2/neu^{low} 4T1 breast tumors. (Scale bar, 50 μm) Three biologically independent animals for each group were tested with similar results.

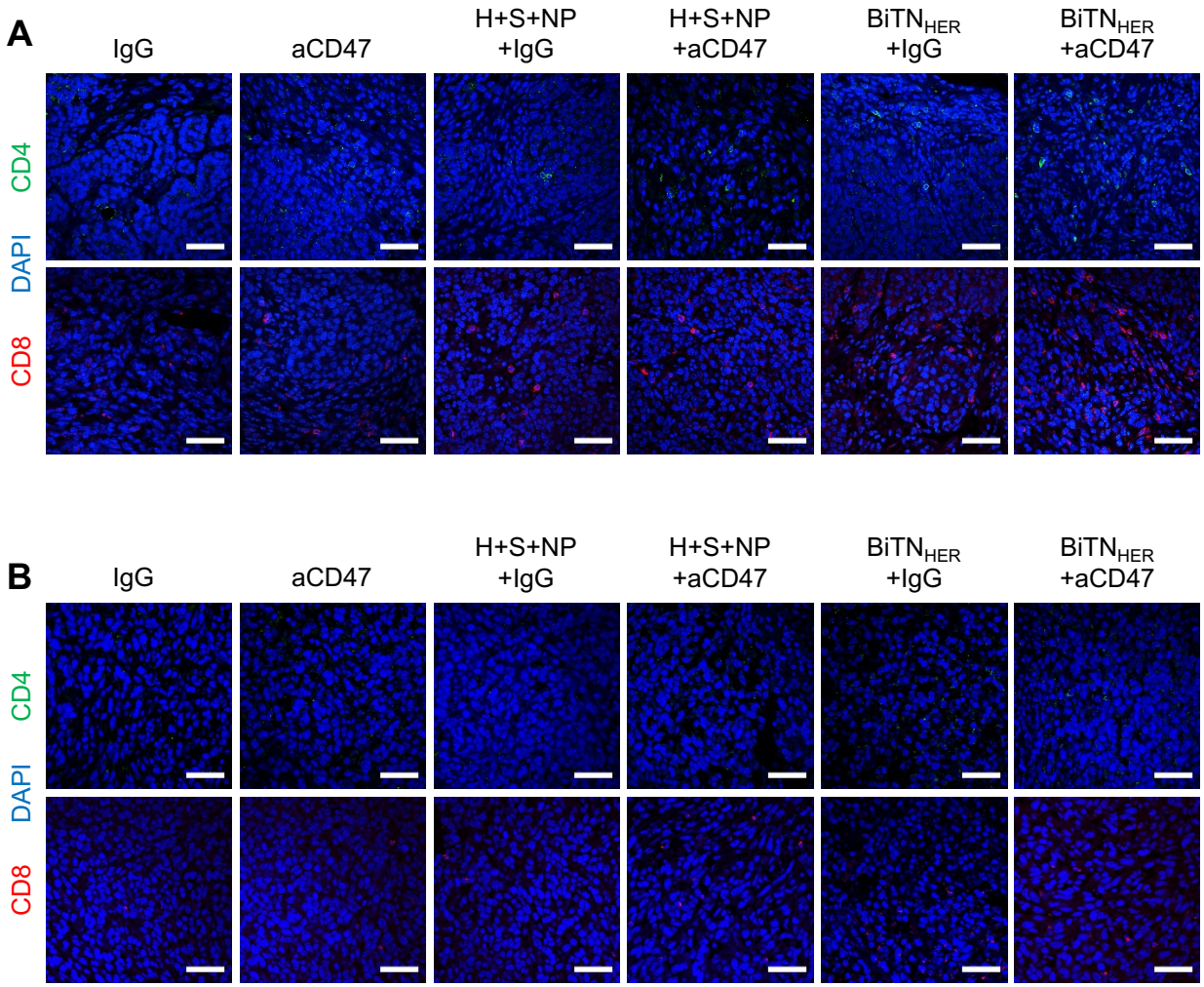

Figure S14. Combined treatment of BiTN$_{HER}$ and aCD47 induced lymphocyte infiltration in a HER2-dependent manner. Combined treatment of BiTN$_{HER}$ and aCD47 increased the CD4^{+}T and CD8^{+}T cell infiltration within (A) HER2/neu^{high} TUBO breast tumors in BALB/c mice, compared with (B) HER2/neu^{low} 4T1 breast tumors. (Scale bar, 50 μm) Three biologically independent animals for each group were tested with similar results.

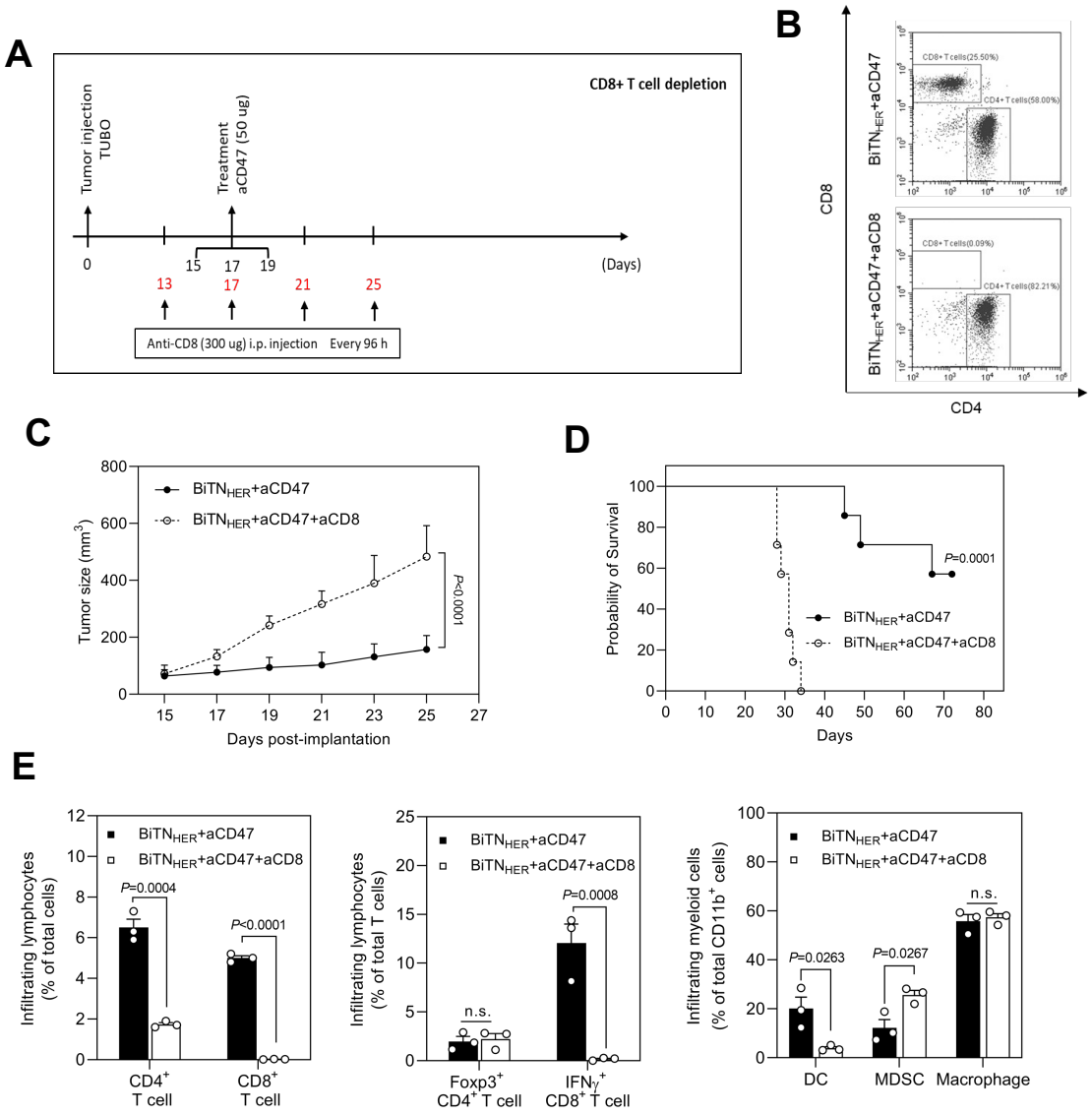

Figure S15. CD8 depletion study. (A) *In vivo* experimental design for CD8 depletion in TUBO tumor-bearing mice. (B) Flow cytometry analysis of splenocytes confirmed that CD8$^+$ T cells were completely depleted after aCD8 treatment. (C) The tumor-inhibitory effect of the combination treatment was abrogated by CD8$^+$ T cell depletion (n=7). (D) The survival benefit for mice was abrogated by CD8$^+$ T cell depletion; ***P<0.001 by log-rank test (n=7). (E) CD8$^+$ T cell depletion significantly decreased the infiltration of CD4$^+$ cells, CD8$^+$ T cells, and dendritic cells (DCs), especially the number of infiltrated IFNγ-producing CD8$^+$ T cells, while increasing the number of immunosuppressive myeloid-derived suppressor cells (MDSCs) (n=3). For all figures, data are presented as mean±s.e.m.. *P<0.05, ***P<0.001, ****P<0.0001 by unpaired Student's t test for the indicated comparisons; n.s., not significant.

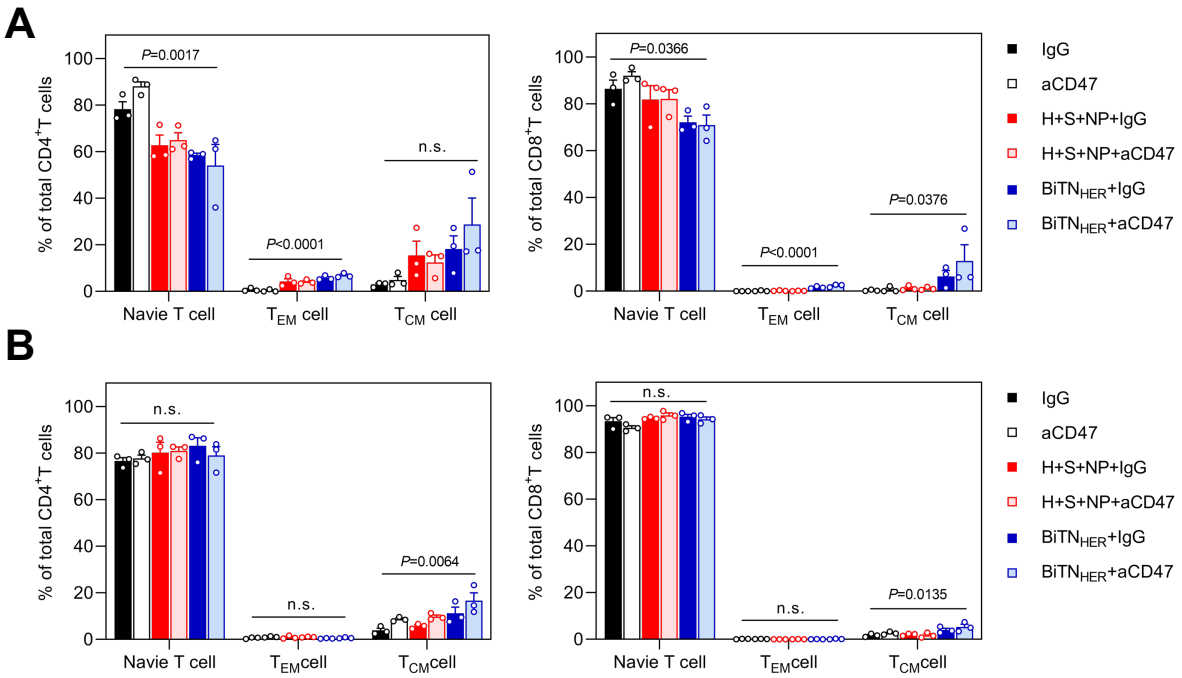

Figure S16. The combination of $BiTN_{HER}$ and aCD47 induced memory T cell activation. (A) Flow cytometric analysis of splenocytes from TUBO tumor-bearing mice showed that the combination of $BiTN_{HER}$ and aCD47 induced a shift in naïve $CD4^+$ and $CD8^+$ T cells towards memory phenotypes (n=3). (B) The combination of $BiTN_{HER}$ and aCD47 induced a shift in naïve $CD4^+$ and $CD8^+$ T cells towards central memory phenotypes, but not effective memory phenotypes (n=3). For all figures, data are presented as mean±s.e.m. **P*<0.05, ***P*<0.01, ****P*<0.001, *****P*<0.0001 by one-way ANOVA with a Bonferroni *post hoc* correction; n.s., not significant.

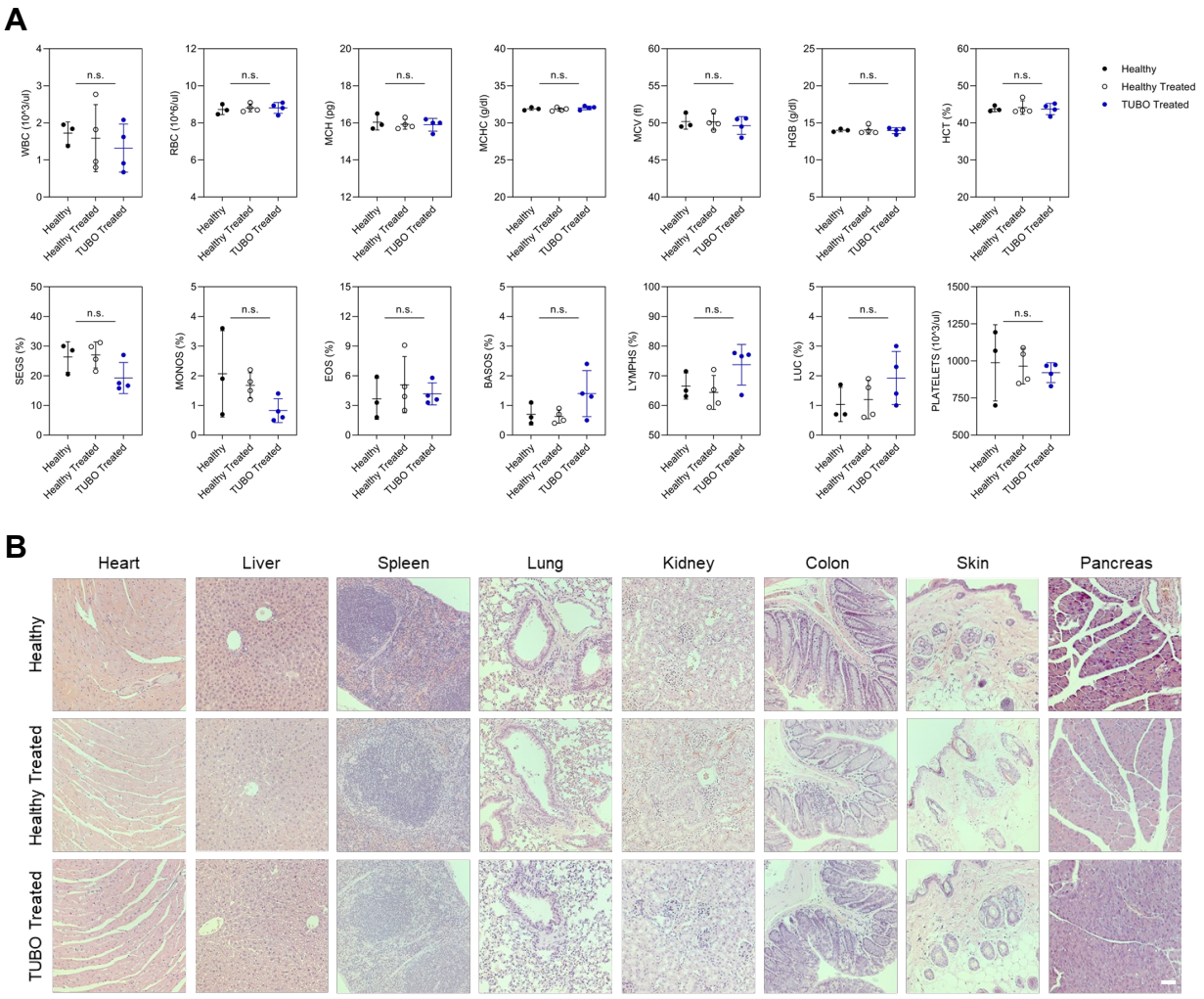

Figure S17. BiTN treatment didn't induce long term autoimmune toxicity. (A) No significant change of complete blood count was observed on mice 30 days after treatment. Healthy, healthy Balb/c mice without treatment; Healthy Treated, healthy Balb/c mice with subcutaneous injection of $BiTN_{HER}$ and aCD47; TUBO Treated, TUBO-bearing Balb/c mice with intratumoral injection of $BiTN_{HER}$ and aCD47 (n=3 for Control group, n=4 for Control Treated and TUBO Treated groups). (WBC, white blood cell; RBC, red blood cell; MCH, mean corpuscular hemoglobin; MCV, mean corpuscular volume; MCHC, mean corpuscular hemoglobin concentration; HGB, hemoglobin; HCT, hematocrit; SEGS, segmental neutrophils; MONOS, monocytes; EOS, eosinophils; BASOS, basophils; LYMPHS, lymphocytes; LUC, large unstained cells). P>0.05, not significant (n.s.). (B) H&E staining of major organs 30 days after the last treatment (scale bar, 1mm). No obvious inflammation or lymphocyte infiltration was observed on mice 30 days after treatment. Healthy, healthy Balb/c mice without treatment; Healthy Treated, healthy Balb/c mice with subcutaneous injection of $BiTN_{HER}$ and aCD47; TUBO Treated, TUBO-bearing Balb/c mice with intratumoral injection of $BiTN_{HER}$ and aCD47. Data are presented as mean±s.e.m. (n=3). *P*>0.5 was seen as not significant (n.s.) by one-way ANOVA with a Bonferroni *post hoc* correction.

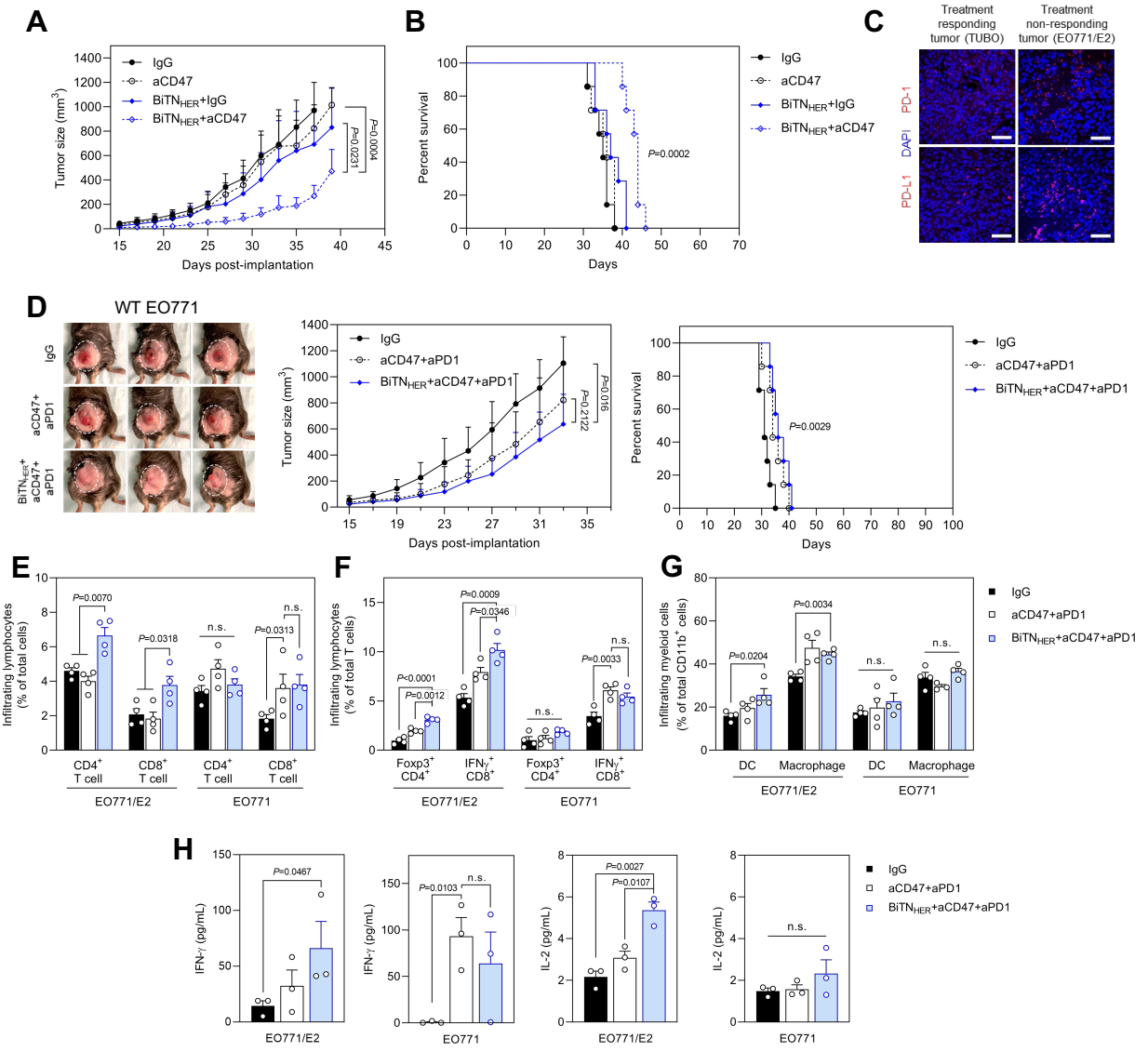

Figure S18. PD1 blockade enhanced the antitumor effect of BiTN$_{HER}$ /aCD47 combination treatment in the more immunosuppressive tumor type EO771/E2. (A) Tumor growth was inhibited by treatment with BiTN$_{HER}$ and aCD47 (n=8) and (B) slightly prolonged the survival of EO771/E2-bearing mice. (C) Immunofluorescence staining showed higher expression of PD1 and PDL1 in the relatively unresponsive tumor type EO771/E2 compared with responding tumor type TUBO (scale bar, 50 μm). Three biologically independent animals for each group were tested with similar results. (D) The triple combination treatment (BiTN$_{HER}$, aDC47, and aPD1) did not suppress tumor growth in EO771-bearing mice (n=7), but did increase the number of infiltrating lymphocytes in EO771/E2 tumors (n=4) (E). (F) The triple combination treatment enhanced infiltration of IFNγ-producing CD8$^+$ T cells and regulatory CD4$^+$ T cells into EO771/E2 tumors (n=4) and increased the infiltration of dendritic cells (DCs) and macrophages in EO771/E2 tumors (n=4) (G). (H) The triple combination treatment increased cytokine levels in the peripheral blood of EO771/E2 tumor-bearing mice (n=3). For all figures, data are presented as mean±s.e.m. *P<0.05, **P<0.01, ***P<0.001 by unpaired Student's t test for the indicated comparisons; ***P<0.001 by log-rank test.

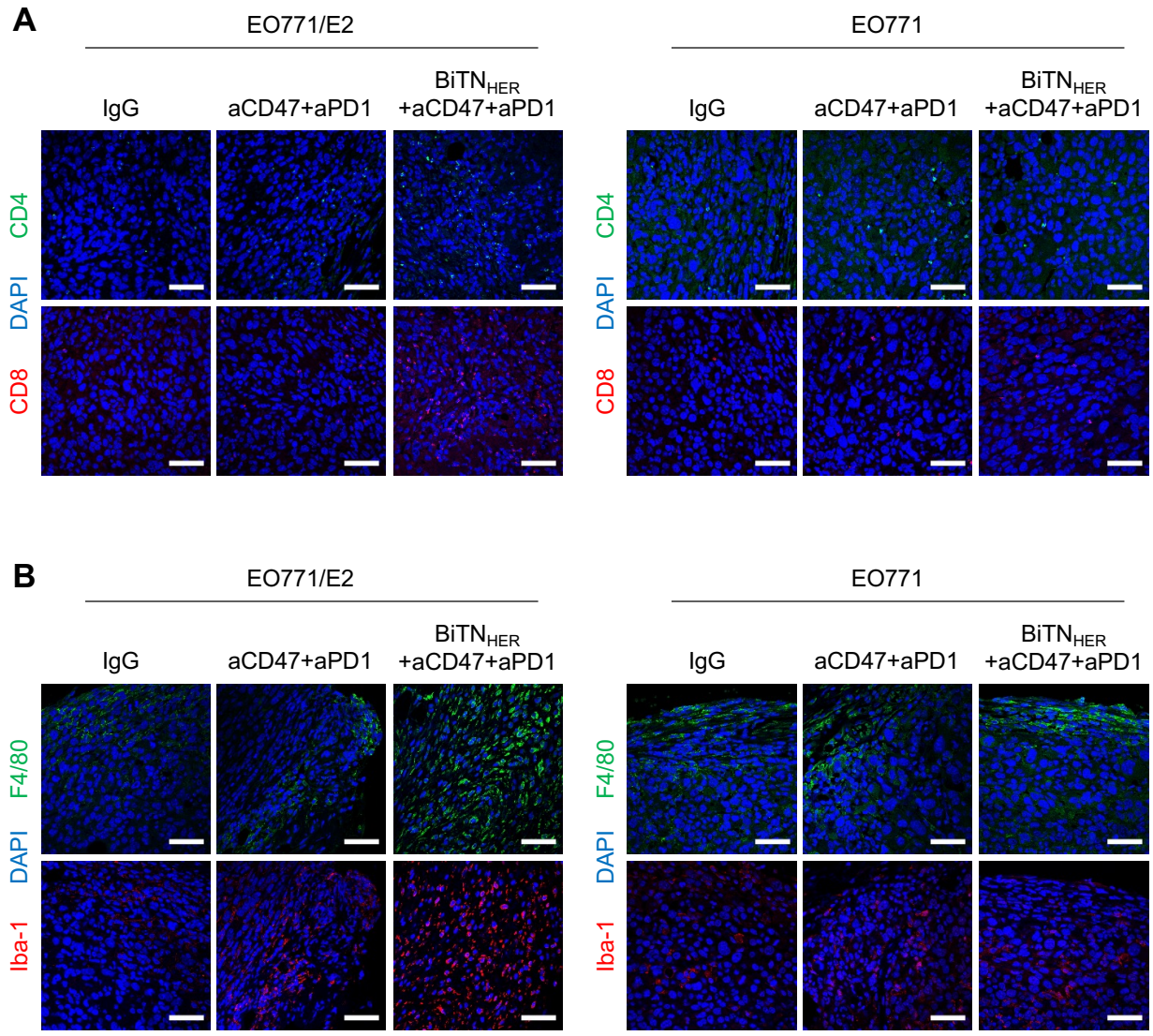

Figure S19. Immunostaining of immune cell infiltration in EO771/E2 and EO771 tumors from C57BL/6 mice. (A) The triple combination treatment (BiTN$_{HER}$ +aCD47+aPD1) increased the infiltration of CD4^{+}T and CD8^{+}T cells within HER2^{high} EO771/E2 breast tumors in C57BL/6 mice, compared with HER2^{low} EO771 breast tumors. (B) The triple combination treatment also increased the infiltration and activation of macrophages within HER2^{high} EO771/E2 breast tumors in C57BL/6 mice, compared with HER2^{low} EO771 breast tumors. (Scale bar, 50 μm) Three biologically independent animals for each group were tested with similar results.

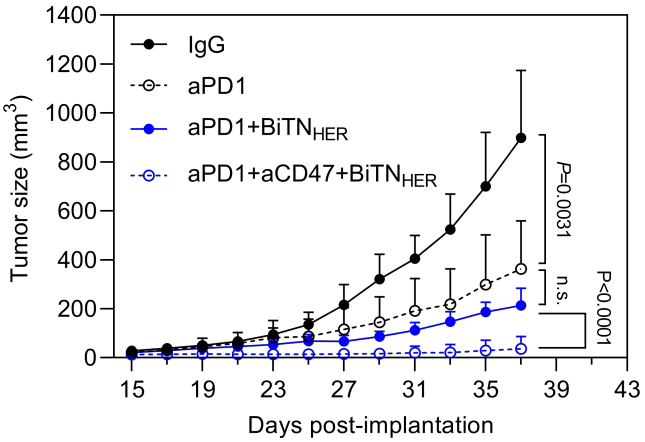

Figure S20. CD47 blockade is required for potent tumor inhibition in EO771/E2 tumor-bearing mice. Combination of aPD1 with $BiTN_{HER}$ retarded rapid tumor growth compared with IgG, but the anti-tumor effect is not as potent as the triple combination treatment of aCD47, aPD1 and $BiTN_{HER}$ (n=6). Data are presented as mean±s.e.m.; ***P*<0.01, *****P*<0.0001 by unpaired Student's t-test for the indicated comparisons; n.s., not significant.

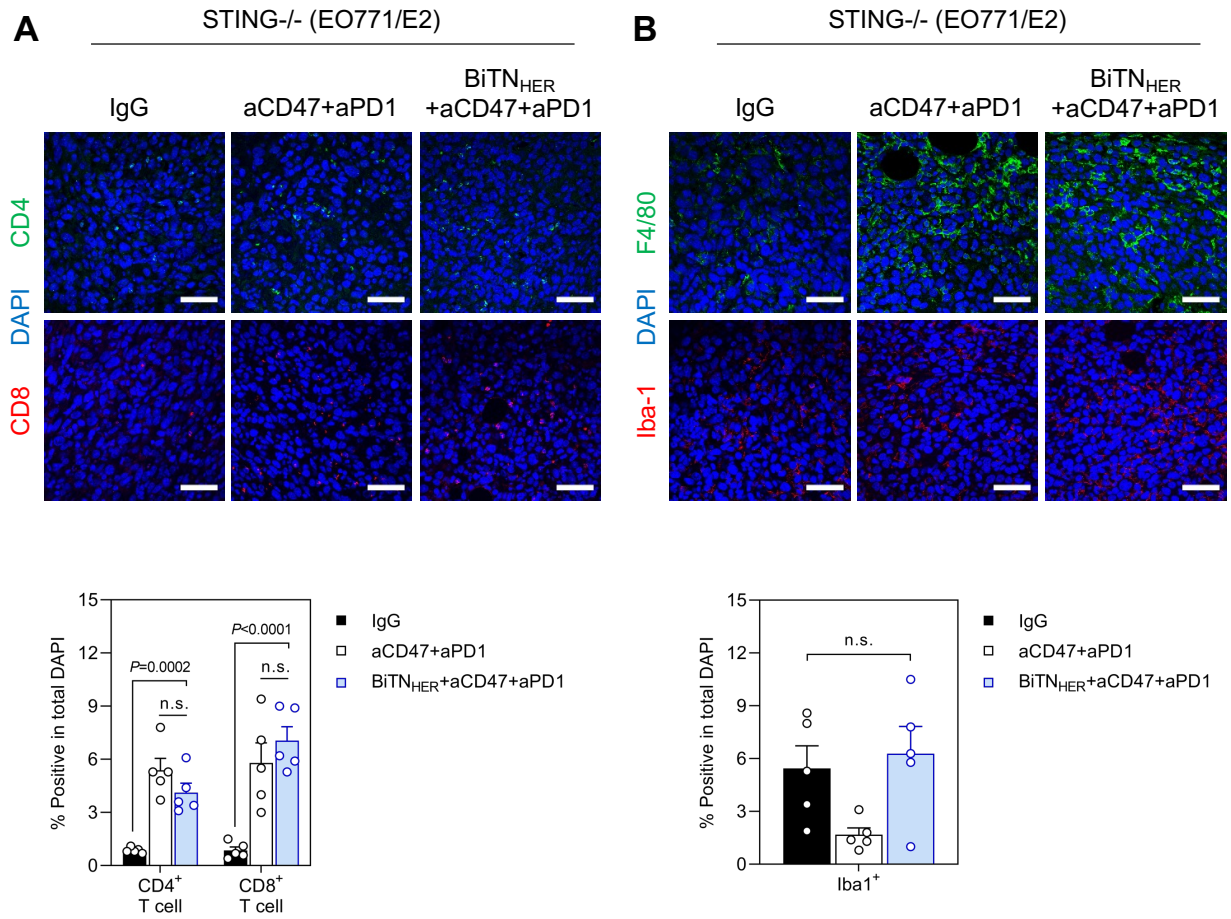

Figure S21. Immunostaining of immune cell infiltration in EO771/E2 and EO771 tumors from STING knockout mice. (A) Treatment with aCD47+aPD1 increased the infiltration of $CD4^+$ and $CD8^+$ T cells into $HER2^{high}$ EO771/E2 breast tumors in STING-knockout mice, but the addition of $BiTN_{HER}$ P had little effect. (B) Combined treatment of $BiTN_{HER}$ and aCD47+aPD1 increased the infiltration of macrophages into $HER2^{high}$ EO771/E2 breast tumors, but not in STING knockout mice. (Scale bar, 50 μm). For all figures, data are presented as mean±s.e.m. (n=5). ***P<0.001, ****P<0.0001 by unpaired Student's t test for the indicated comparisons; n.s., not significant.

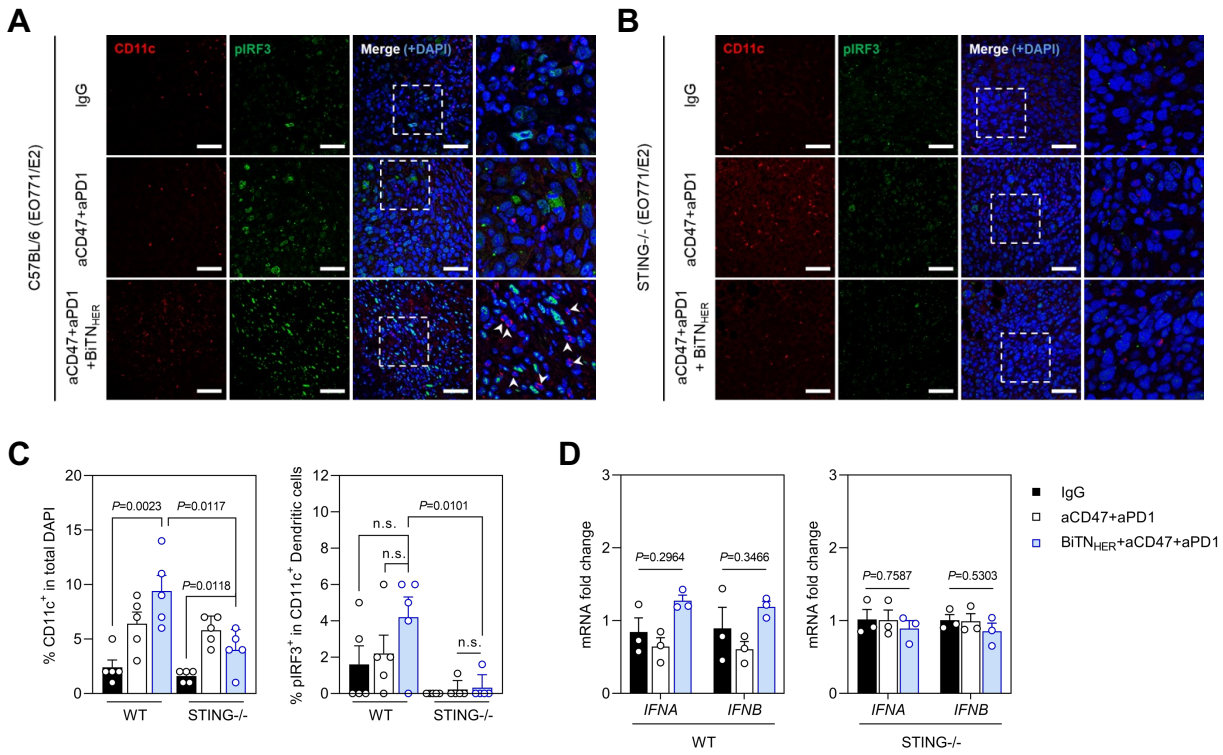

Figure S22. STING signaling was not activated in dendritic cells during combination treatment. (A-B) Immunofluorescence staining of EO771/E2 tumors implanted in WT (A) and STING knockout (B) mice; areas within the dashed squares are shown at higher magnification to the right; arrowheads indicate the nuclear translocation of pIRF3 within CD11c$^+$ dendritic cells (scale bar, 50 μm). (C) Quantification of infiltrated CD11c$^+$ DCs and percentage of nuclear pIRF3$^+$ DCs in the tumors (n=5). (D) Expression of type I interferons was not significantly elevated in intratumoral CD11c$^+$ macrophages after the triple combination therapy (*IFNA*, interferon α; *IFNB*, interferon β) (n=3). For all figures, data are presented as mean±s.e.m. **P*<0.05, ***P*<0.01 by unpaired Student's *t* test for the indicated comparisons; n.s., not significant.

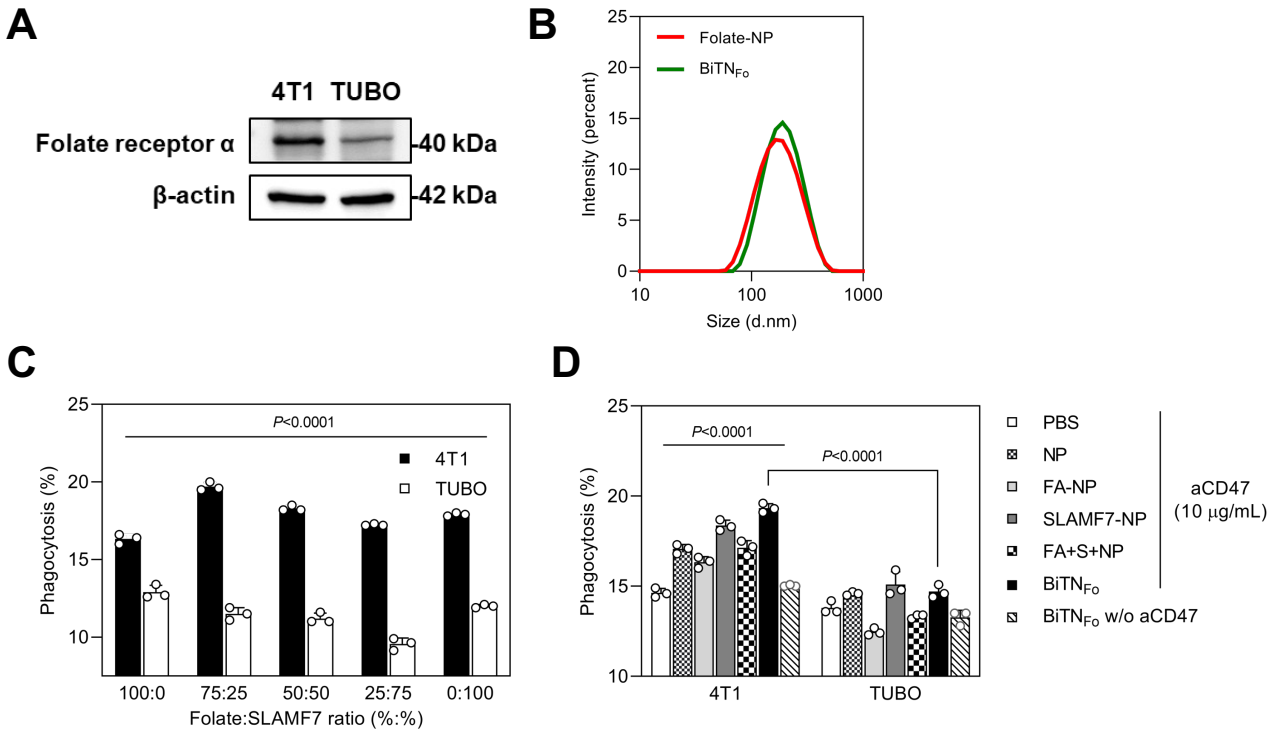

Figure S23. Enhanced macrophage phagocytosis in a folate receptor–targeted manner. (A) The triple-negative breast cancer cell 4T1 expresses higher levels of folate receptor (FR) α than does the TUBO cell line. (B) Size distribution of folate-conjugated nanoparticles (Folate-NP) and folate/SLAMF7-conjugated nanoparticles (BiTN$_{Fo}$) measured by diffuse light scattering. (C) BiTN$_{Fo}$ at a 3:1 folate:SLAMF7 conjugation ratio had the most robust pro-phagocytic effect in FR^{high} 4T1 cancer cells. (D) Similarly, BiTN$_{Fo}$ transformed FR-expressing 4T1 mouse breast cancer cells into SLAMF7^{high} cells and promoted mouse (BALB/c bone marrow) macrophage phagocytosis in the presence of aCD47. Data are presented as mean±s.e.m. (n=3). ****P<0.0001 by one-way ANOVA with a Bonferroni *post hoc* correction; ****P<0.0001 by unpaired Student's t test for the indicated comparisons.

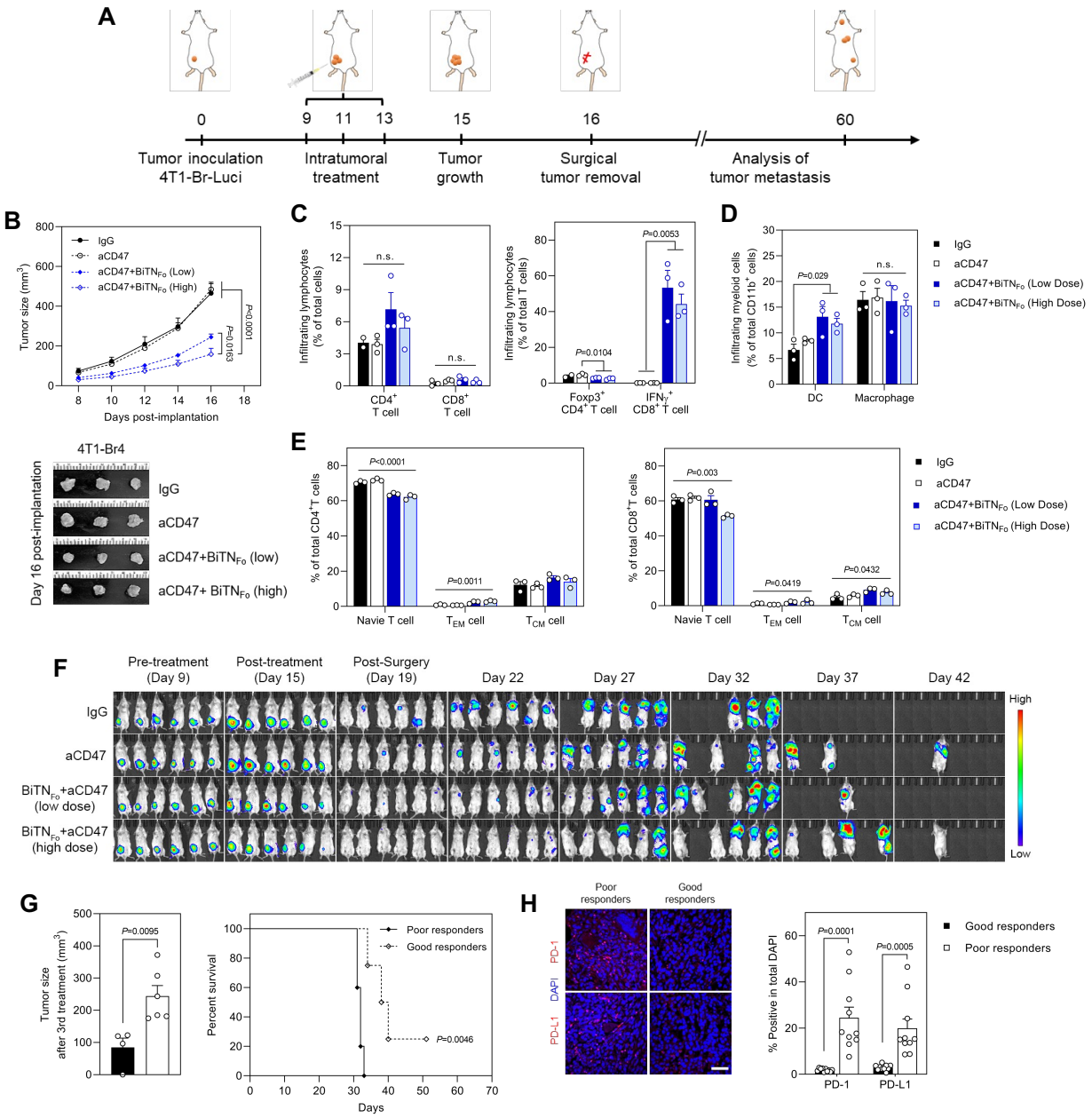

Figure S24. Combination treatment with BiTN$_{Fo}$ and aCD47 did not induce an efficient systemic antitumor effect in 4T1 tumor metastasis owing to PD1 expression. (A) Experimental design for establishing 4T1 tumor metastasis model and treatment. (B) The BiTN$_{Fo}$ +aCD47 combination treatment inhibited primary tumor growth in 4T1-bearing BALB/c mice (n=6). (C) The BiTN$_{Fo}$ +aCD47 combination treatment significantly increased the infiltration of IFNγ-producing CD8$^+$ T cells and decreased the number of intratumoral regulatory T cells in the primary 4T1 tumor (n=3). (D) Combined BiTN$_{Fo}$ and aCD47 treatment promoted the infiltration of professional antigen-presenting dendritic cells (DCs) (n=3). (E) Flow cytometric analysis of splenocytes from 4T1 tumor-bearing mice showed that BiTN$_{Fo}$ +aCD47 induced a shift in naïve CD4$^+$ and CD8$^+$ T cells towards memory phenotypes (n=3). (F) The BiTN$_{Fo}$ +aCD47 combination treatment induced the fewest and smallest tumor metastases after surgical removal of the primary tumor. (G) Tumor size after the 3rd treatment with BiTN$_{Fo}$ +aCD47 for good responders vs poor responders (n=3); good responders survived longer than did poor responders (poor: n=5, good: n=4). (H) PDL1 and PD1 levels were significantly lower in the tumor microenvironment of good responders to the

combination treatment. For all figures, data are presented as mean±s.e.m. *P<0.05, **P<0.01, ****P<0.0001 by one-way ANOVA with a Bonferroni *post hoc* correction; *P<0.05, **P<0.01, ***P<0.001, ****P<0.0001 by unpaired Student's *t* test for the indicated comparisons; **P<0.01 by log-rank test; n.s., not significant.

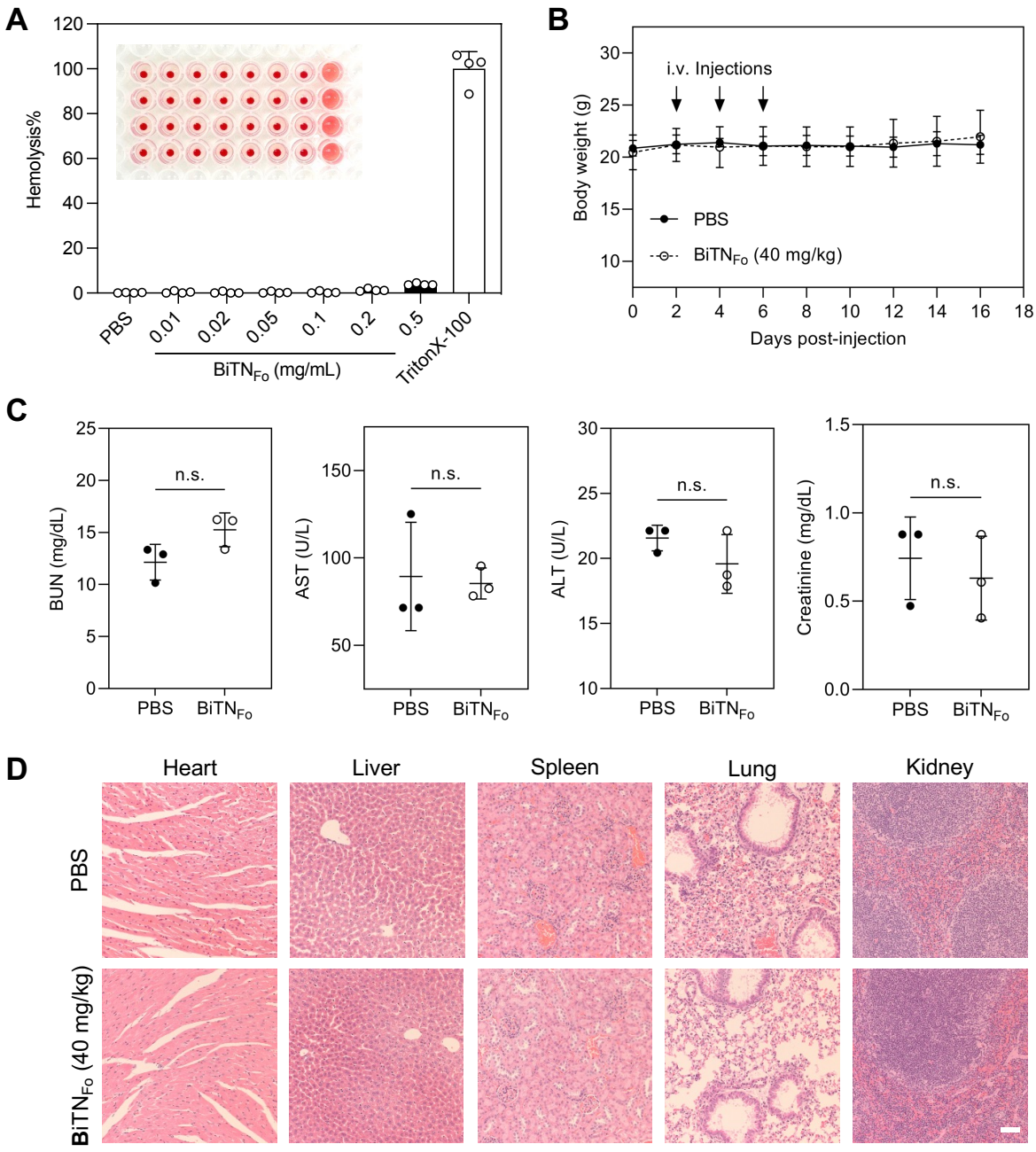

Figure S25. Biocompatibility of BiTN$_{Fo}$. (A) No obvious hemolysis was observed after *in vitro* incubation of erythrocytes with BiTN$_{Fo}$ within the range of estimated blood concentrations of BiTN$_{Fo}$ after intravenous injection at 40 mg/kg (n=4). (B) No significant change in body weight was observed after intravenous injection of BiTN$_{Fo}$ (n=3). (C) Intravenous injection of BiTN$_{Fo}$ did not significantly change the peripheral blood levels of urea nitrogen (BUN), aspartate aminotransferase (AST), alanine aminotransferase (ALT),

or creatinine (n=3). (D) Intravenous injection of $BiTN_{Fo}$ did not show obvious toxicity to major organs (scale bar, 1 mm). Three biologically independent animals for each group were tested with similar results. For all figures, data are presented as mean±s.e.m.; *P*>0.5 was seen as not significant (n.s.) by one-way ANOVA with a Bonferroni *post hoc* correction.

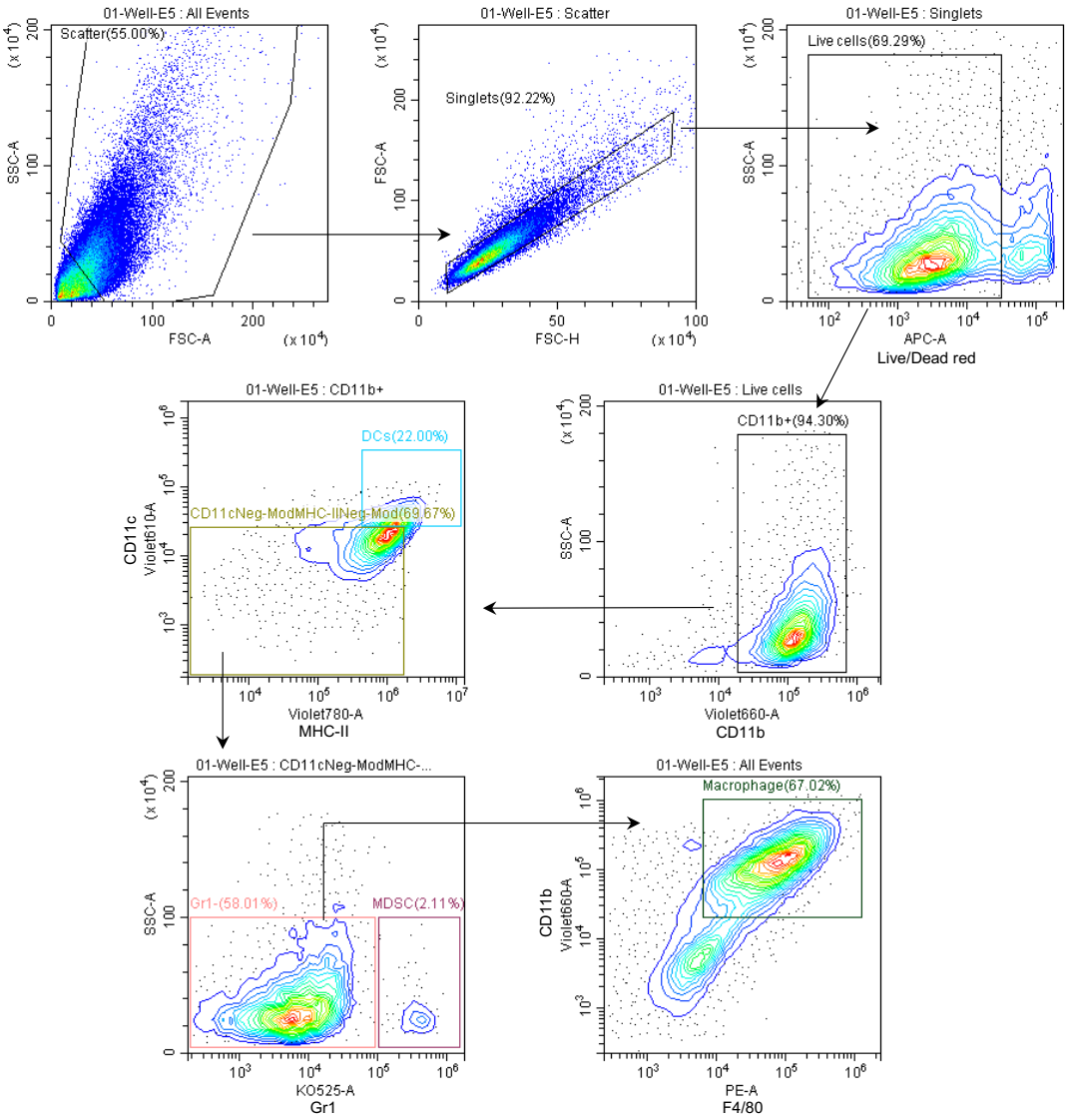

Figure S26. Gating strategy for analyzing myeloid cells, including dendritic cells (DCs), myeloid-derived suppressor cells (MDSCs) and macrophages from CD45-selected cells from tumors related to Figures 3 and 5 and Supplementary Figures S15, S18, and S24.

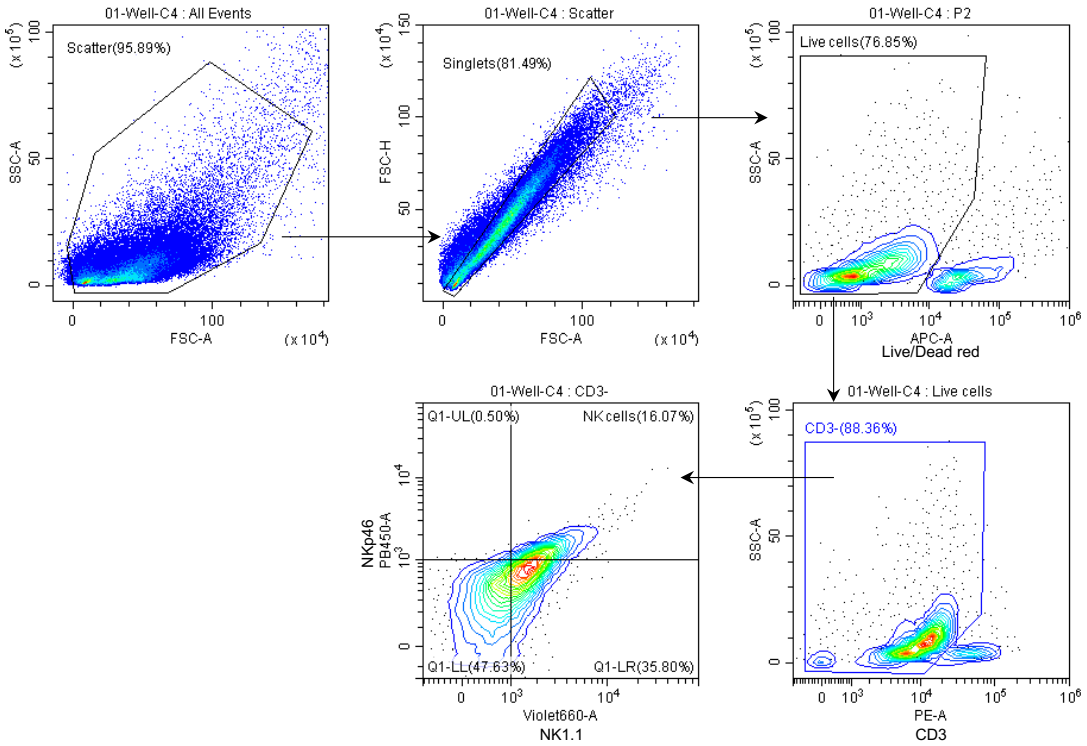

Figure S27. Gating strategy for analyzing NK cells from CD45-selected cells from tumors related to Supplementary Figures S12.

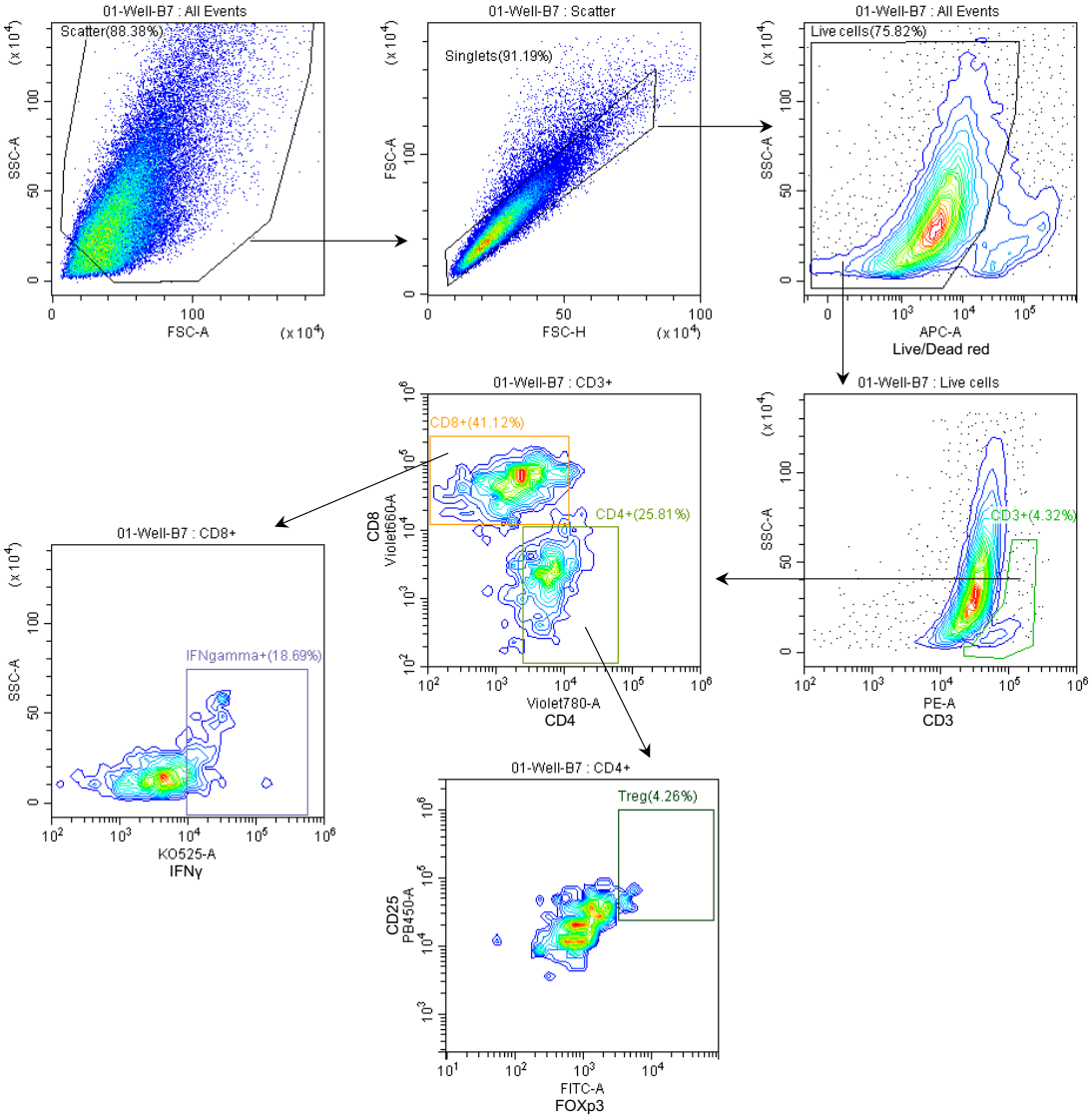

Figure S28. Gating strategy for analyzing T cells from CD45-selected cells from tumors related to Figures 3 and 5 and Supplementary Figures S15, S18, S24.

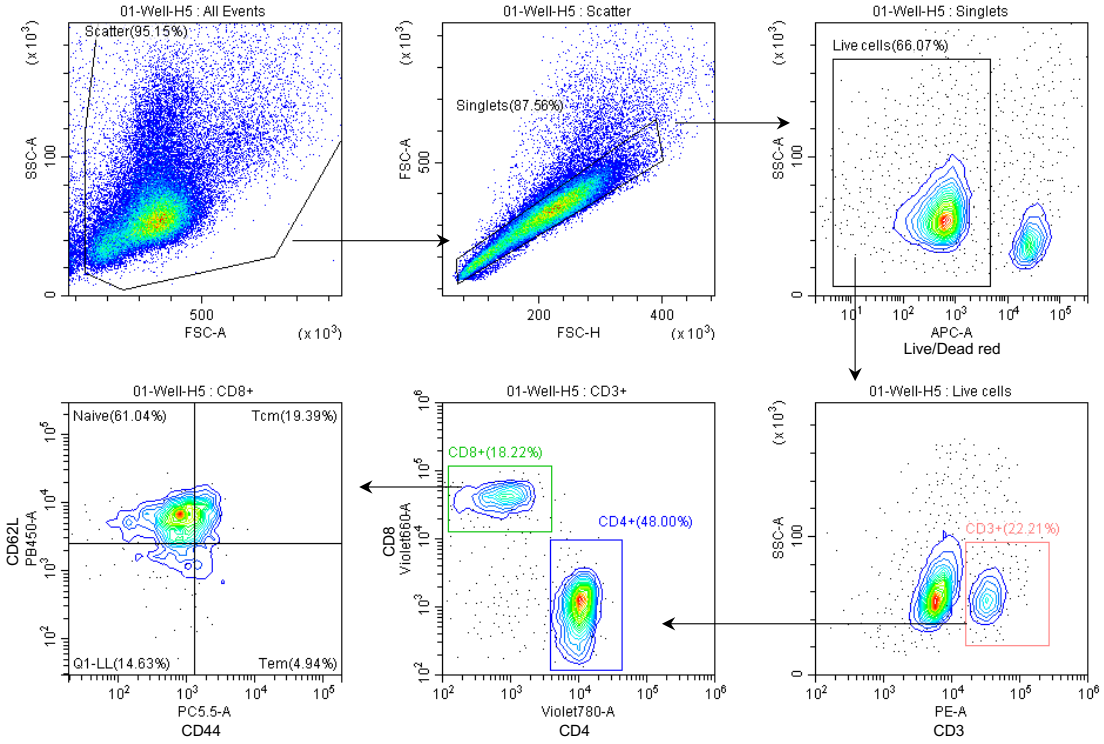

Figure S29. Gating strategy for analyzing splenocytes from spleens related to Supplementary Figures S16 and S24.

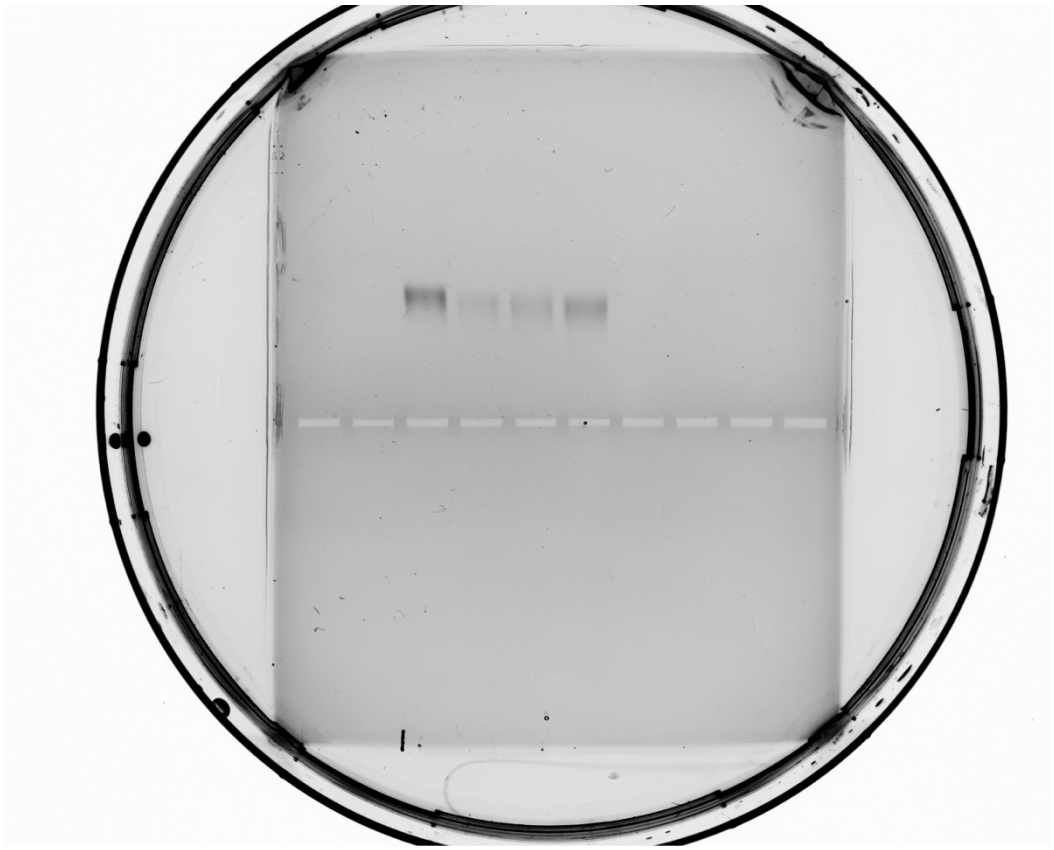

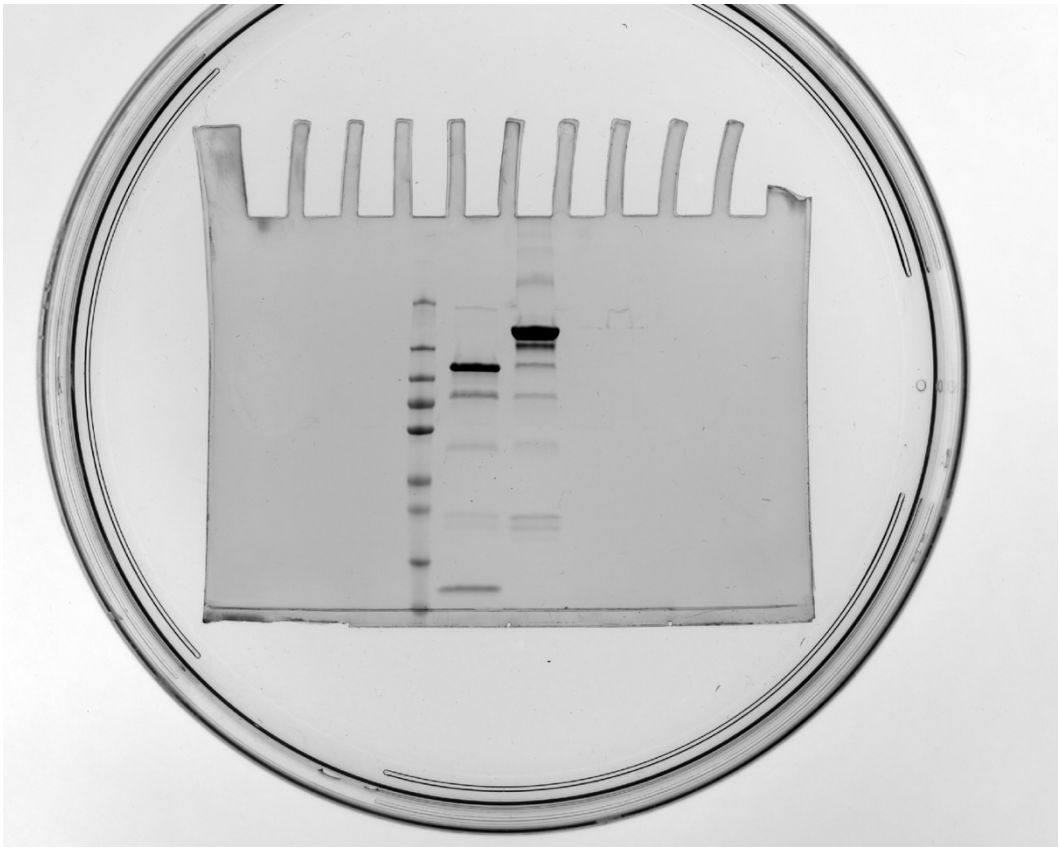

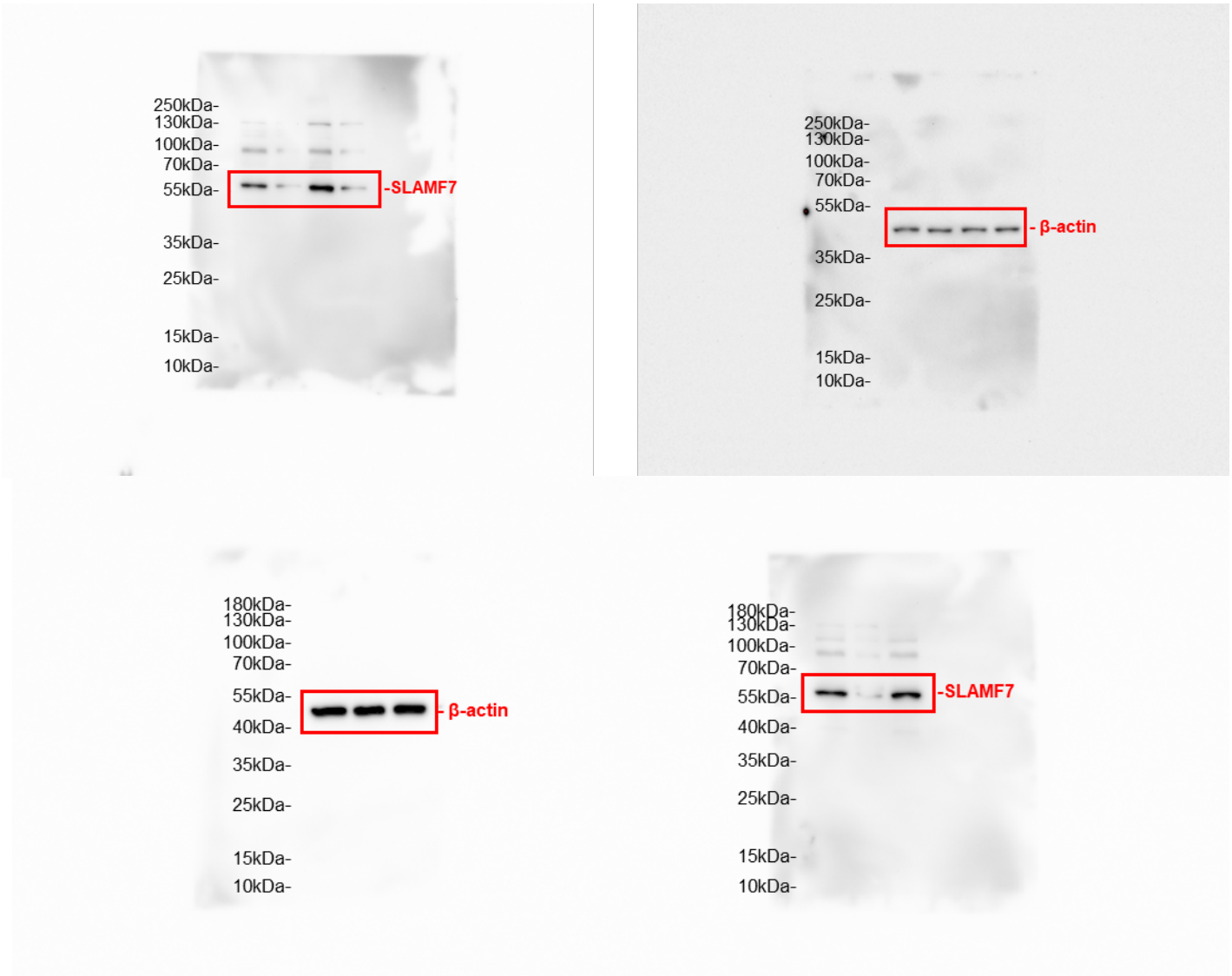

Figure S30. Uncropped original gel images of western blots in Figure 1c, S4, S9, S23.